TRANSPORTATION POOLED FUND PROGRAM
QUARTERLY PROGRESS REPORT

Lead Agency (FHWA or State DOT): ____Maryland Department of Transportation_____

INSTRUCTIONS:
Project Managers and/or research project investigators should complete a quarterly progress report for each calendar quarter during which the projects are active. Please provide a project schedule status of the research activities tied to each task that is defined in the proposal; a percentage completion of each task; a concise discussion (2 or 3 sentences) of the current status, including accomplishments and problems encountered, if any. List all tasks, even if no work was done during this period.

Transportation Pooled Fund Program Project # *TPF-5(285)*	**Transportation Pooled Fund Program - Report Perio** □Quarter 1 (January 1 – March 31) □Quarter 2 (April 1 – June 30) □Quarter 3 (July 1 – September 30) ■Quarter 4 (October 1 – December 31)

Project Title:
Standardizing Lightweight Deflectometer Measurements for QA and Modulus Determination in Unbound Bases and Subgrades

Name of Project Manager(s): Rodney Wynn	**Phone Number:** 443-572-5043	**E-Mail** RWynn@sha.state.md.us
Lead Agency Project ID: TPF-5(285)	**Other Project ID (i.e., contract #**	**Project Start Date:** January/15/2014
Original Project End Date: December/31/2015	**Current Project End Date:** December/31/2015	**Number of Extensions:** 0

Project schedule status:
□ On schedule □ On revised schedule □ Ahead of schedule ■ Behind schedule

Overall Project Statistics:

Total Project Budget	Total Cost to Date for Projec	Percentage of Work Completed to Date
$371,984	**$118,522.63**	**41%**

Quarterly Project Statistics:

Total Project Expenses and Percentage This Quarter	Total Amount of Funds Expended This Quarter	Total Percentage of Time Used to Date
$ 27,182.18 **7.3%**	**$ 27,182.18**	**41%**

Progress this Quarter (includes meetings, work plan status, contract status, significant progress, etc.):

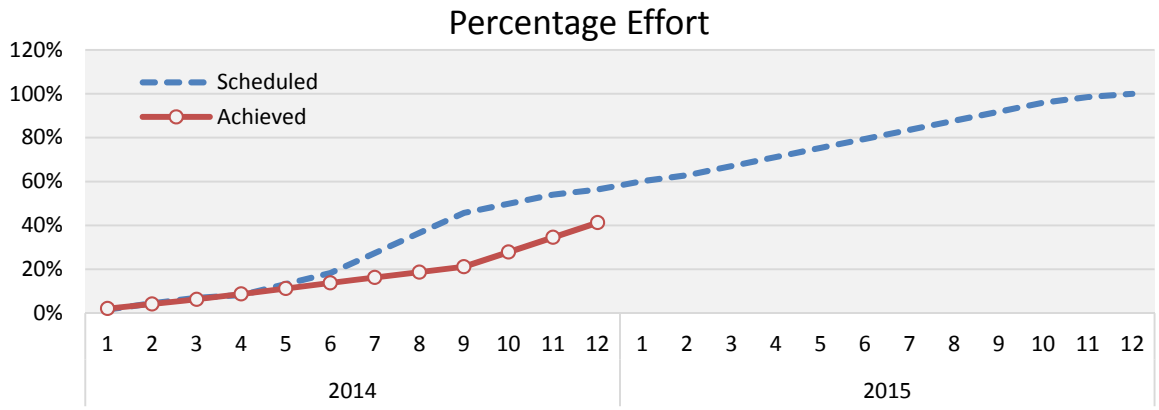

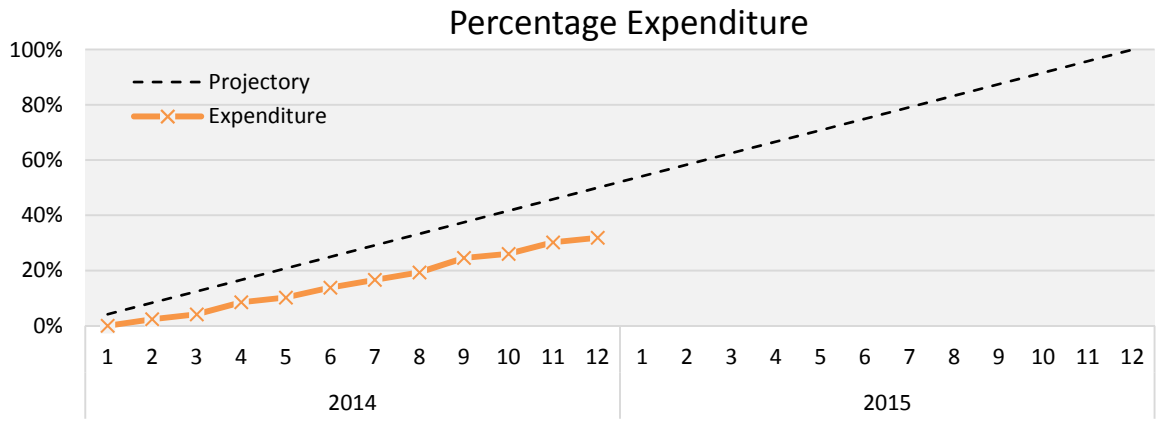

The progress with respect to each Task is as followed:

Task 1. Literature Review (3.3% of the total effort). Percent completion: 100%

The personnel continue the review of the current and upcoming literature when deemed necessary.

Project personnel participating in these activities: Schwartz, Khosravifar, Afsharikia.

Task 2. Equipment Evaluation (2.4% of the total effort). Percent completion: 100%

All the LWDs were received and are being evaluated.

MB45 Ohaus Moisture Analyzer was evaluated in the laboratory against oven-drying measurements. The MB45 takes about 15 minutes to dry the samples vs. considerably longer times in the oven. The results show a very high correlation (R = 0.98) between the moisture contents measured using the two techniques. The moisture content measured by MB45 is generally slightly lower (approximately 0.9 times) than the moisture measured using the oven drying technique. Results from the evaluation are summarized in Appendix A. Our conclusion is that the MB45 a robust device, especially for fine soils. The few drawbacks of the MB45 are: 1) Its low capacity makes it less suitable for larger aggregates; and 2) The need for a generator to power the

device in the field.

Task 3. Model Refinement/Development (12.6% of the total effort). Percentage completion: 86%

The principal activities/findings under Task 3 during the reporting period include the following:

a. Several models for incorporating the effects of soil suction on resilient modulus have been evaluated. Preliminary results from this investigation are summarized in a paper accepted for the ASCE Airfield and Highway Pavement Conference in Miami in June; this paper is attached as Appendix B. The Lytton 1995 model for resilient modulus was found the more accurate model in terms of considering the effects of suction and degree of saturation. Investigations are continuing on some newer models and other soil databases.

b. The frequency domain analysis of LWD impact load on the Beam Verification Tester (Task 4) ihas been implemented in MATLAB. This step is necessary for evaluating the full spectral response of different LWDs and any inherent differences that may lead to systematic discrepancies or errors in the field.

c. During the previous quarter we tried to simulate moisture loss in soil using the HYDRUS 1D model and software. The volumetric water content profile for two types of one-layered soils (clay and top soil) were comparable to the laboratory measured tests performed by Yanful and Choo (1997). However, HYDRUS 1D did not perform well for two layered soil systems. Due to an unknown software malfunction, the water content results did not vary with changing input parameters such as initial moisture content and meteorological conditions. There was also a discrepancy in the initial moisture content of about 3% for the layered soil analyses. The software bugs are being investigated.

   To continue modeling the drying of a layered soil, soil evaporation mechanisms have been studied in more detail to understand better the underlying concepts (Appendix C). A new code UNSAT-H (based on Gupta et al. 1978) was identified as being applicable to this study. The UNSAT-H model simulates liquid water flow using the Richards equation, water vapor diffusion using Fick's law, and sensible heat flow using the Fourier equation. We are currently evaluating the capability of UNSAT-H and HYDRUS to predict the moisture profile of compacted soil during drying process, especially for layered soil systems.

d. The nonlinear structural pavement algorithm proposed in NCHRP 10-84 final report is being assessed/modified for setting the field target moduli.

e. The suitability of performing laboratory LWD tests on Proctor molds for QA is being assessed. This approach might be a good practical substitute for laboratory resilient modulus testing to determine appropriate target stiffness values. Details of this assessment to date are summarized in Appendix D.

Project personnel participating in these activities: Schwartz, Khosravifar, Afsharikia.

Task 4. Controlled Trials (18.8% of the total effort). Percentage completion: 61%

Laboratory LWD tests on Proctor Compacted Specimens: During a meeting with Mr. Larry Olson, CEO of Olson Engineering, he recommended executing LWD drops on Proctor compacted soils during AASHTO T99 or AASHTO T180 compaction.

LWD tests on Proctor molds were performed on 4 soils obtained from the field projects (Task 5). The procedure and preliminary findings from this work are detailed in Appendix D.

In summary the process is as follows: The samples were prepared using Standard Proctor test (AASHTO T99). The tests were performed for 4 different scenarios:

1. Right after compaction directly on the Proctor molds. LWD drops using a plate diameter matching the Proctor mold are performed concurrent to compaction moisture-density curve establishment. The modulus-moisture curves are superimposed on the compaction density-moisture curves.
2. Drying process after compaction at OMC. Replicate samples are compacted to OMC-MDD using Standard Proctor energy. LWD tests (one at each sample) are performed: (a) immediately after compaction, (b) after 8 hours of drying, and (c) after 24 hours of drying in a controlled environmental chamber.
3. Drying process after compaction at OMC+2%. Replicate samples are compacted to wet of optimum (OMC+2%) using constant energy according to AASHTO T99 resulting in lower density. LWD tests (one at each sample) are performed: (a) immediately after compaction, (b) after 8 hours if drying, and (c) after 24 hours of drying in a controlled environmental chamber.
4. Drying process after compaction at OMC-2%. Replicate samples are compacted to dry of optimum (OMC-2%) using constant energy according to AASHTO T99 resulting in lower density. LWD tests (one at each sample) are performed: (a) immediately after compaction, (b) after 8 hours of drying, and (c) after 24 hours of drying in a controlled environmental chamber.

The elastic modulus of soil was calculated based on theory of elasticity simulating a uniform static load on cylinder of elastic material with constrained lateral movement.

Important findings from the results to date include:

1. As expected, there is a decrease in modulus by an increase in moisture content.
2. The slope of modulus reduction is very steep around the OMC point of the compaction curve.
3. As expected, fine-grained soils show a significantly higher variation in modulus due to moisture variations than do coarse-grained soils.
4. The curve of modulus vs. drying moisture content matches fairly well with the modulus vs. compaction moisture content curve, especially for fine soils. This implies that the effect of short-term moisture variations (post compaction drying), which is one of the main variables during QA, is similar to the influence of compaction moisture content on modulus. This implies that the modulus of the material is not very sensitive to density.

The capabilities of resilient modulus models (Lytton 1995, Cary & Zapata, and others) to predict the LWD measurements on the Proctor mold are being evaluated. The suitability of using LWD measurements during Proctor compaction curve establishment to set the target modulus for field QA is being evaluated.

Laboratory resilient modulus tests: The UTM-100 testing equipment is finally up and running using two external LVDTs and a small 6kN load cell. Due to a manufacturing defect, the load cell became detached on the first attempts with the device after its set up on October 30th. The process of sending it back for repair delayed the resilient modulus testing during this quarter.

Beam Verification Tester (BVT): The static stiffness of the beam was measured at different span length using an INSTRON machine. LWD tests were performed on Olson, Zorn and Dynatest LWDs with different plate sizes and drop heights (if applicable) and at various beam spans. The objective of using BVT is to assess any systematic error in the static stiffness calculated by each LWD test device on a steel beam with known stiffness properties.

During LWD testing on the BVT, dropping the falling weight from the full height of the device usually caused a physical instability leading to “jumping” of the LWD after the impact load (also reported in Hoffmann 2004). This results in the detachment of LWD from the beam system during the load rebound. Two alternative

solutions investigated were to: (1) reduce the impact load on the devices with load cells by dropping the weight from a lower height or using a rubber hammer to induce the impact load directly on the LWD plate; (2) designing a new clamping system to assure more stability in the LWD-Beam structure. The first approach is not a true representation of the LWD device and is not applicable to all kinds of LWDs. Even with LWDs with load cells (e.g., Olson LWD), using a rubber hammer or dropping the weight from a lower height did not provide enough impact to be measured by the sensors. Therefore, the second approach was chosen. The clamping design is now modified to assure better stability.

The spectral analysis procedure was developed in MATLAB. Due to the detachment of LWD-beam system during the load rebound in the previous design, time series had to be truncated before analysis, which impaired the data quality needed for spectral analysis.

The tests will be re-performed on the new modified beam setup during the next quarter.

Controlled soil box tests: The process of signing a Memorandum of Understanding between UMD and TFHRC FHWA has been very prolonged. The tests on the controlled soil box is therefore postponed to the spring.

Project personnel participating in these activities: Schwartz, Khosravifar, Afsharikia, Tefa.

Task 5. Field Validation (53.7% of the total effort). Percentage completion: 25%

LWD testing was performed on four projects in Maryland during the past quarter. Materials were also obtained for laboratory testing (Task 4). The projects are as followed:
US 29: Location Columbia, MD – Base layer (GW: Well-graded gravel with sand)
MD 404: Location Denton, MD – Subgrade (SP-SM: Poorly-graded sand with silt)
MD 424: Location Crofton, MD – Two different Subgrade (SM: silty sand; and SC: clayey sand)
Georgia Ave: Location Silver Spring, MD – Base layer (GW: Well-graded gravel with sand)

The tests included modulus measurements by at least one of the evaluated LWDs (Zorn, Olson LWD, Dynatest), nuclear gauge moisture and density measurements, and Geogauge. The preliminary results are provided in Appendix E.

There was a fairly good correlation between the Zorn LWD (300mm) and Olson LWD (200mm). As expected, there was no an apparent correlation between measured stiffness and density. The models and techniques studied in Task 3 and 4 are being used to adjust the moisture influence on. Further analysis on the field data will be resumed as soon as the resilient modulus test data is obtained.

Task 6. Draft Test Specifications (3.3% of the total effort). Percentage completion: 0%

No progress was made on this task during the reporting period.

Task 7. Workshop and Final Report (5.8% of the total effort). Percentage completion: 0%

No progress was made on this task during the reporting period.

UMD personnel contact information:

1. Charles W. Schwartz- Principal Investigator, 301-405-1962, schwartz@umd.edu
2. Sadaf Khosravifar- GRA, 530-531-5030, sadafkh@umd.edu
3. Zahra Afsharikia- GRA, 202-747-4121, nafshari@umd.edu

Anticipated work next quarter:

- The continued monitoring and documentation of the literature. In particular, new papers presented at TRB 94th annual meeting will be reviewed.
- Task 3, 4, and 5 will be the main focus of the next quarter.
  1. Laboratory resilient modulus testing.
  2. Parametric study using UNSAT-H program.
  3. Evaluation of LWD devices using BVT and spectral analysis
  4. Test pit construction
  5. More rigorous investigation of field results using the laboratory resilient modulus and LWD measurements.
  6. Model refinement
  7. Arrangements with the technical advisory committee for the potential field projects in each state (Task 5).

Circumstance affecting project or budget. (Please describe any challenges encountered or anticipated that might affect the completion of the project within the time, scope and fiscal constraints set forth in the agreement, along with recommended solutions to those problems).

The main circumstance affecting the project has been the installation of the triaxial resilient modulus test unit. The newly purchased load cell became detached due to a manufacturer flaw right after installation on October 30th. The time required for sending it back for repair further delayed the resilient modulus testing. The machine is now in working condition.

The test pit evaluation is postponed due to the prolonged process of obtaining a signed MOU and because of weather conditions.

Field projects have also encountered cancelations due to weather conditions as winter approached.

Potential Implementation:

LWDs should be implemented more widely and this should be done using standardized testing procedures and data interpretation methods. LWDs are tools for performance based construction quality assurance testing that not only result in a better product but also provide the quantitative measures critical to better understanding the connection between pavement design and long term pavement performance. As the benefits of performance based quality assurance testing become increasingly apparent, more public agencies and private consultants are expected to acquire these tools and implement standardized procedures during their use. The product of this research will allow state DOT construction specifications to be modified to include this new LWD option for construction quality assurance.

Appendix A

MB45 Ohaus Moisture Analyzer Evaluation

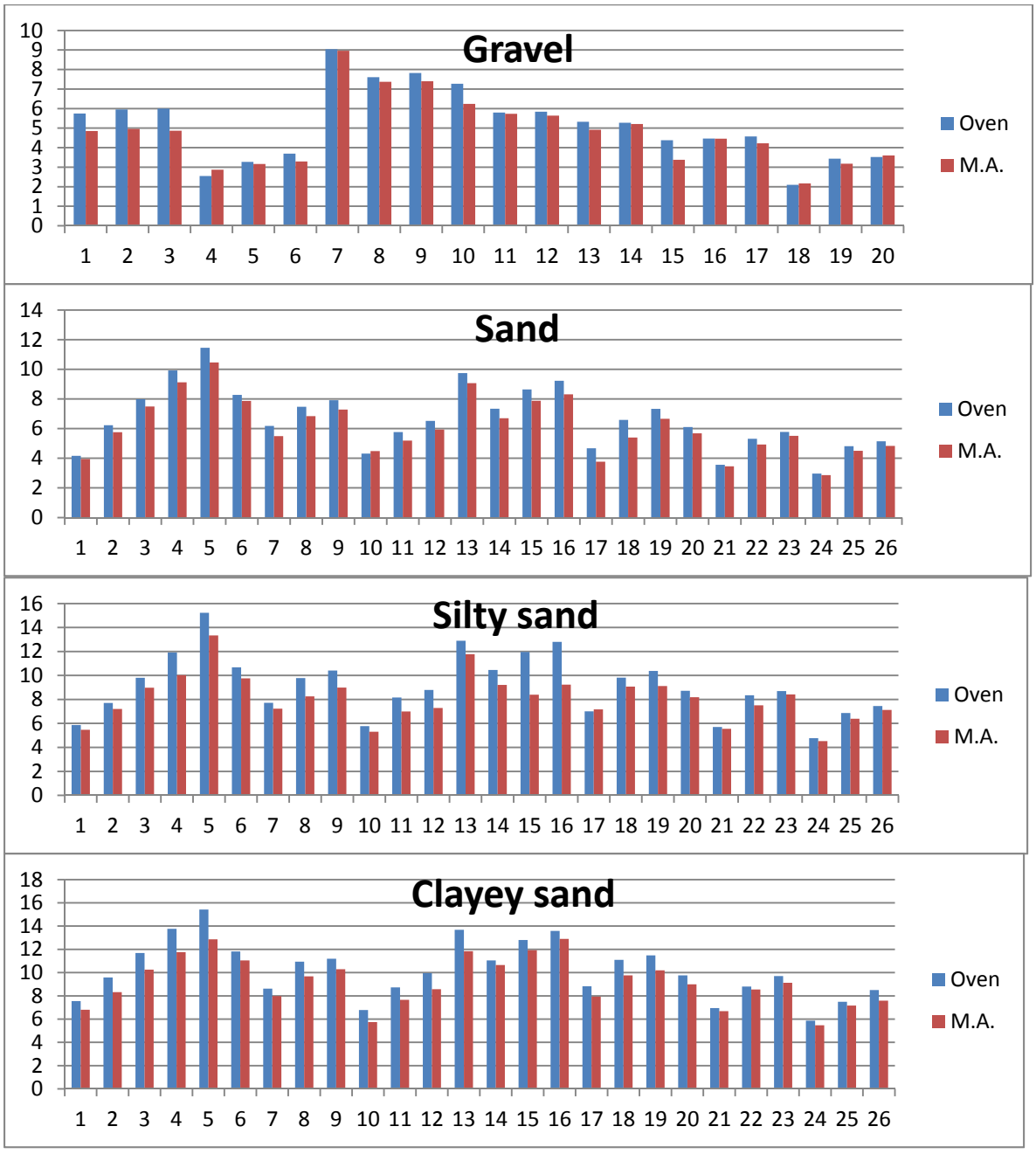

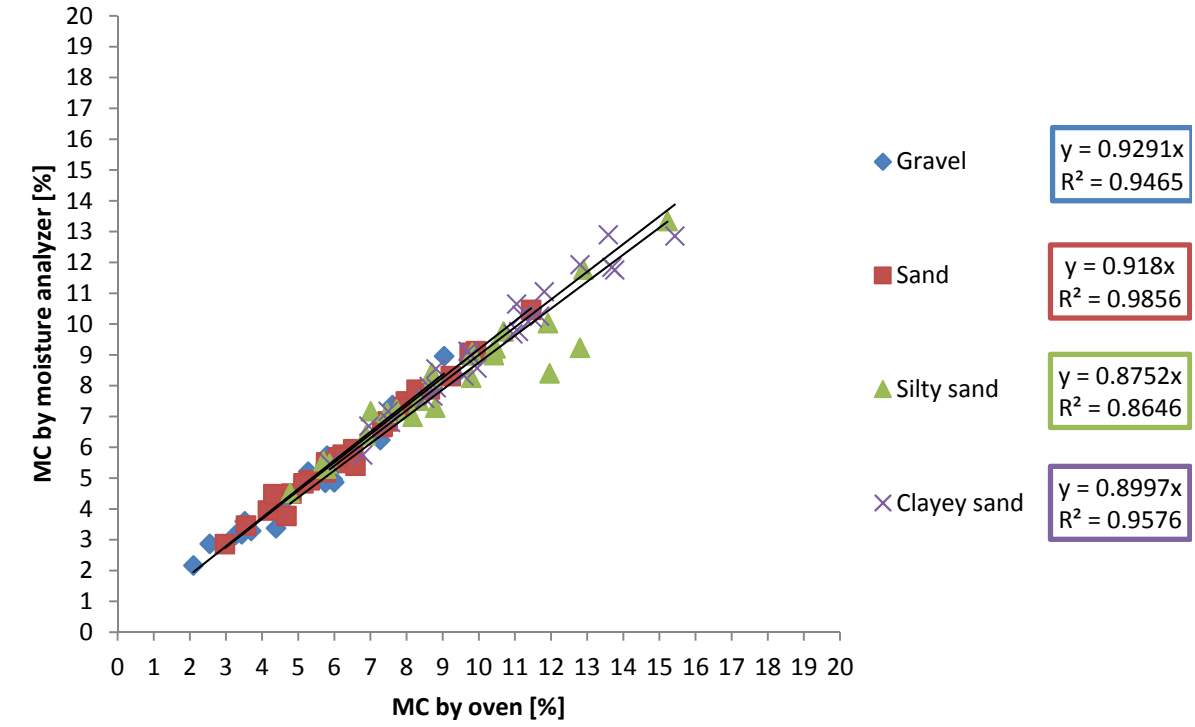
MC by moisture analyzer [%]
MC by oven [%]
Gravel
Sand
Silty sand
Clayey sand
y = 0.9291x
R² = 0.9465
y = 0.918x
R² = 0.9856
y = 0.8752x
R² = 0.8646
y = 0.8997x
R² = 0.9576

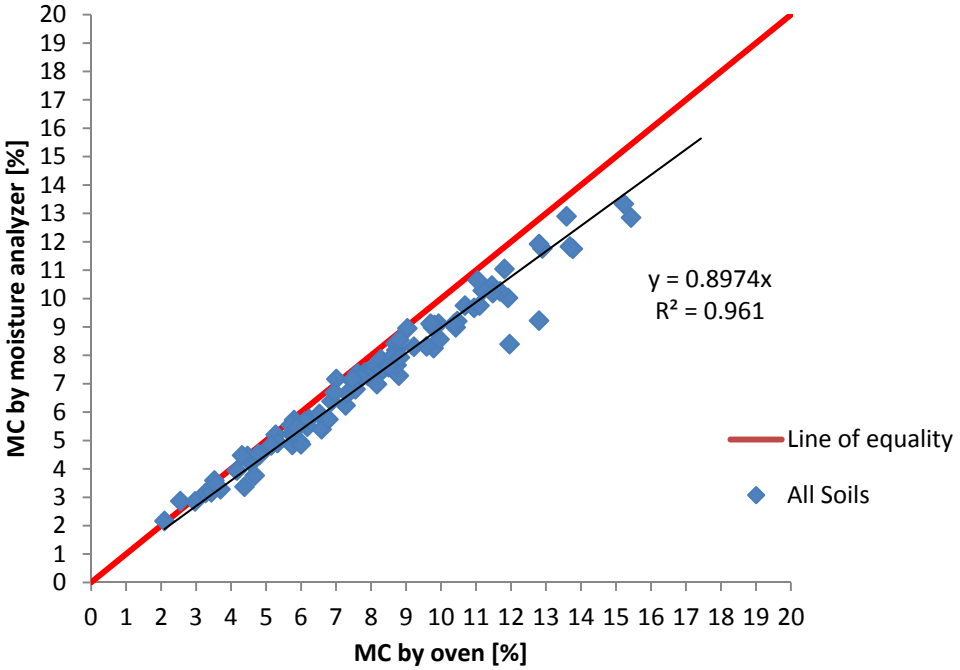
MC by moisture analyzer [%]
MC by oven [%]
y = 0.8974x
R² = 0.961
Line of equality
All Soils

Appendix B.

Khosravifar, S., Afsharikia, Z., and Schwartz, C.W. (2015). “Evaluation of Resilient Modulus Prediction Models for Cohesive and Noncohesive Soils.” Submitted to the ASCE Airfield and Highway Pavement Conference, Miami, June. (accepted)

Evaluation of Resilient Modulus Prediction Models for Cohesive and Noncohesive Soils

Sadaf Khosravifar[1], Zahra Afsharikia[2], Charles W. Schwartz[3]

[1]Department of Civil and Environmental Engineering, University of Maryland, 1173 Glenn L. Martin Hall, College Park, MD, 20742; PH (530) 531-5030; FAX (301) 405-2585; email: sadafkh@umd.edu
[2]Department of Civil and Environmental Engineering, University of Maryland, 1173 Glenn L. Martin Hall, College Park, MD, 20742; PH (202) 747-4121; FAX (301) 405-2585; email: nafshari@umd.edu
[3]Department of Civil and Environmental Engineering, University of Maryland, 1173 Glenn L. Martin Hall, College Park, MD, 20742; PH (301) 405-1962; FAX (301) 405-2585; email: schwartz@umd.edu

ABSTRACT

Geomaterials are often in unsaturated condition during their service life and their resilient modulus is influenced by several factors including moisture content, density, void ratio, plasticity, and etc. There are various constitutive models to predict the nonlinear resilient modulus of unbound materials as a function of the aforementioned factors—particularly moisture and stress states based on empirical equations or theoretical unsaturated soil mechanics concepts.

In this study, seven existing constitutive models and two predictive models were evaluated using eight different soil databases with different properties including cohesive and non-cohesive soils. The constitutive models were calibrated based on the data at optimum moisture content and maximum dry density. Consecutively, the calibrated models were used to predict the resilient modulus at other moisture or density conditions. The models were compared in terms of their rationality, accuracy of prediction, and applicability to the widest range of soils.

INTRODUCTION

Resilient modulus (M_R), a measure of stiffness, is a fundamental material property for unbound pavement materials. It is the most important material input for subgrade and base soils required by Mechanistic—Empirical Pavement Design Guide (MEPDG). The resilient modulus for an individual soil can significantly vary with changes in density, moisture content, gradation, plasticity index, and the stress levels (Vanapalli et al., 1999). Uzan (1985) proposed a nonlinear constitutive model based on the bulk and octahedral shear stresses.

For soils in saturated or unsaturated conditions, the mechanical response is a function of effective stresses rather than total stresses (Bishop, 1960; Terzaghi, 1996). In unsaturated soils, two main factors form the effective stresses; (1) pore air pressure (u_a) which is often insignificant, and (2) the difference between u_a and the pore water pressure (u_w), designated as matric suction ($u_a - u_w$) or simply u as referred to in this

study. Bishop (1960) formulated the effective stress of unsaturated soils as shown in equation 1.

$$\sigma' = (\sigma - u_a) + \chi(u_a - u_w) \quad (1)$$

Matric suction (u) is a function of pore size geometry, pore size distribution, and the soil water content and can be predicted from soil-water characteristic curve (SWCC) (Fredlund and Xing, 1994). The effective stress parameter (χ)—also known as pore suction resistance factor—in Equation 1 is a material variable that shows the contribution of the matric suction in the effective stress and is generally considered to vary between zero and unity, corresponding to a completely dry and fully saturated condition, respectively. At the fully saturated condition, the equation reduces to Terzaghi's classic effective stress equation.

While several researchers e.g. Lytton (1995), Khalili and Khabbaz (1998), Roberson and Siekmeier (2002) have proposed different models to quantify the pore suction resistance factor, these have not been well accepted to date and χ equal to 1 is often preferred by researchers (Morgenstern, 1979).

To characterize the nonlinear modulus of soils, tests at various conditions—in particular stress and moisture—may be required. Yet, routine testing is usually only performed at optimum moisture and density condition. Therefore, implementation of an accurate constitutive model based on mechanics of unsaturated soils capable of predicting the nonlinear M_R at other moisture and density conditions is a necessity. In this study several resilient modulus constitutive models and two empirical predictive models were evaluated on independent cohesive and noncohesive soils. The models were compared in terms of their rationality, accuracy of prediction, and applicability to the widest range of soils.

MATERAL PROPERTIES

In this study, 4 types of subgrade and 4 types of granular base soil data from Andrei (2003) were used to evaluate the models. The soil type and description for each material is presented in Table 1. More information about the volumetric and mechanical properties of the soils can be found in Andrei (2003).

Table 1- Soil Type and Description (From Andrei, 2003)

	SOIL TYPES	DESCRIPTION
Subgrade	Phoenix Valley Subgrade (PVSG)	Clayey Sand, SC
	Yuma Sand Subgrade (YSSG)	Poorly Graded Gravel with Sand, GP, Non Plastic
	Flagstaff Clay Subgrade (FCSG)	Clayey Sand, SC
	Sun City Subgrade (SCSG)	Clayey Sand, SC
Base	Grey Mountain Base (GMAB2)	Well Graded Gravel with Sand, GW, Non Plastic
	Salt River Base (SRAB2)	Poorly Graded Sand with Gravel, SP, Non Plastic
	Globe Base (GLAB2)	Poorly Graded Sand with Silt and Gravel, SP-SM, Non Plastic
	Prescott Base (PRAB2)	Poorly Graded Sand with Silt and Gravel, SP-SM, Non Plastic

All base materials and one of the subgrade soils were non-plastic. The soil water characteristic curves, which were key inputs to the evaluated models, were predicted from the gradation and soil indices using the Fredlund and Xing (1994) procedure. The unconfined compression (U_C), which was input to one of the predictive models, was estimated from CBR values according to Black (1962).

For all of the soils, the M_R test was performed on specimens compacted with standard and modified proctor, at their corresponding optimum moisture content as well as above and below optimum. This resulted in a total of 6 scenarios for each soil.

EVALUATED MODELS

Several predictive and constitutive models have been proposed by previous researchers to model the resilient modulus of soils; 9 have been selected here for evaluation. The parameters of the following models were calibrated—except for M4 and M6 predictive models—based on the measured data at optimum moisture content and maximum dry density of standard compaction test scenario. The models where subsequently used to predict the M_R at the other moisture-density conditions. The evaluated models are explained below:

M1 is the general nonlinear model implemented in the MEPDG and is a function of total bulk stresses. This model does not consider the effect of suction *u*.

$$\textbf{M1}: M_R = K_1 P_a \left(\frac{\sigma_{bulk}}{P_a}\right)^{K_2} \left(\frac{\tau_{oct}}{P_a} + 1\right)^{K_3} \quad (2)$$

in which $\sigma_{bulk} = \sigma_1 + \sigma_2 + \sigma_3 = \sigma_d + 3\sigma_c$, $\sigma_1, \sigma_2, \sigma_3 =$ three principal stresses, σ_d= deviatoric stress, σ_c= confining stress, τ_{oct}= octahedral shear stress = $\frac{\sqrt{3}}{2}\sigma_d$, and the coefficients K_1, K_2, and K_3 are regression coefficients.

M2, the second evaluated model, is similar to M1, with the bulk effective stress ($\sigma_{bulk} + 3u$) replacing σ_{bulk}. The reason for the multiplication of suction by 3 is that suction adds to each of the three principal effective stresses.

$$\textbf{M2}: M_R = K_1 P_a \left(\frac{\sigma_{bulk}+3u}{P_a}\right)^{K_2} \left(\frac{\tau_{oct}}{P_a} + 1\right)^{K_3} \quad (3)$$

M3, proposed by Liang et al (2008) adds a suction dependency term (χ) to the effective stress term. The suction dependency term was proposed by Khalili and Khabbaz (1998). In this model the suction term (u) is not multiplied by 3.

$$\textbf{M3}: M_R = K_1 P_a \left(\frac{\sigma_{bulk}+\chi u}{P_a}\right)^{K_2} \left(\frac{\tau_{oct}}{P_a} + 1\right)^{K_3} \quad (4)$$

$$\chi = \left(\frac{(u_a - u_w)_b}{u_a - u_w}\right)^{0.55} = \frac{u_{air-entry}}{u} \quad (5)$$

The $u_{air-entry}$ term is the suction at air entry level where air starts to enter the largest pores in the soil. The upper limit of χ is equal to 1.

M4, proposed by Siekmeier (2011), has been found a suitable predictive model for subgrade and fine soils. The K_1-K_3 coefficients are also predicted as a function of suction and volumetric moisture content from SWCC of the soils. The equations are shown as followed:

$$M_R = K_1 P_a \left(\frac{\sigma_{bulk} + \theta_w f u}{P_a}\right)^{K_2} \left(\frac{\tau_{oct}}{P_a} + 1\right)^{K_3} \quad (6)$$

in which $K_1 = 800 \times \left(\frac{1}{5\theta_{sat}}\right)^{1.5} \times \left(\frac{1}{log_{10}(u)}\right)$, $K_2 = log_{10}(u) - 1$, $K_3 = -8\theta_{sat}$, $f = \theta_w^{10\theta_{sat}^3}$, θ_w= volumetric water content, θ_{sat}= volumetric water content at saturation, and $\chi = \theta_w f$.

The χ in M4 model is not bracketed by the upper bound of 1. The M4 predictive model was re-evaluated as model M5, in which the K values were calibrated for each soil through nonlinear regression. The formula for *f* was kept the same.

Yan et al. (2013) proposed two predictive models for subgrade soils based on gene expression programming (GEP) to correlate M_R with routine properties of subgrade soils and state of stress. GEP I was computationally unstable for nonplastic soils and was found erroneous for plastic soil and has thus been excluded from the comparisons. The GEP II model, selected for evaluation as model M6—is displayed below:

M6: $M_R = \text{atan}\left\{\gamma_d * \left[\frac{\gamma_d - U_c}{PI}\right]\right\} + \left\{2 * \left[\frac{sqrt(PI)}{P_{200}}\right]\right\} + \sigma_d + \left\{2 * \sin\left[\frac{\gamma_d * \exp\{\text{atan}[\sin(P_{200})]\}}{P_{200}}\right]\right\} + (\sigma_d * \text{atan}\{sqrt(P_{200}) - [(\sigma_d * P_{200})/\gamma_d]\}) + \{\text{atan}[sqrt(U_c) - \gamma_d] + \text{atan}(\gamma_d)\}$ (7)

in which U_c = unconfined compressive strength, *PI* = Plasticity Index, *P200* = percentage passing the No. 200, γ_d= dry density, and σ_d= deviatoric stress.

Recently, Gu et al. (2014) evaluated a model proposed by Lytton (1995) and reported satisfactory predictions for base course aggregates. The model is:

$$M_R = K_1 P_a \left(\frac{\sigma_{bulk} - 3\theta_w f u}{P_a}\right)^{K_2} \left(\frac{\tau_{oct}}{P_a}\right)^{K_3} \quad (8)$$

The *f* parameter in this model is a function of θ_a and θ_u, which are volumetric water content of the soil at air entry and unsaturation, respectively. Parameter *f* is bracketed by the upper and lower bounds below:

$$f_{upper\ bound} = \left[\left(\frac{\theta_a - \theta_w}{\theta_a - \theta_u}\right) + \frac{1}{\theta_w}\left(\frac{\theta_w - \theta_u}{\theta_a - \theta_u}\right)\right] \quad (9)$$

$$f_{lower\ bound} = \left[\frac{1}{\left(\frac{\theta_a - \theta_w}{\theta_a - \theta_u}\right) + \theta_w\left(\frac{\theta_w - \theta_u}{\theta_a - \theta_u}\right)}\right] \quad (10)$$

Three *f* values were evaluated in the Lytton model to predict the resilient modulus, resulting in the following models. $\chi = \theta_w f$ ranges from $\theta_u$to 1 and therefore is theoretically sound.

M7 based on $f = \frac{f_{upper\ bound} + f_{lower\ bound}}{2}$
M8 based on $f = f_{upper\ bound}$
M9 based on $f = f_{lower\ bound}$

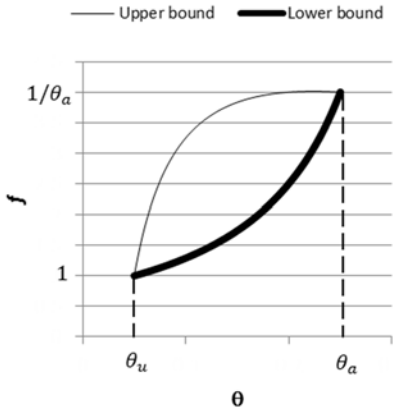

Figure 1. The bounds of pore suction for Lytton (1995).

RESULTS

Least squares analysis was applied to the measured data at optimum moisture content and maximum standard dry density for all models except for the M4 and M6 predictive models to find the best model.

To evaluate the performance of the models, the root mean square error (RMSE) and average relative error (RE) of model prediction were calculated at each moisture condition (Wet, Dry, Optimum), each compaction energy effort (standard and Modified proctor compaction effort), and overall for each soil and every model. RMSE, a measure of model accuracy, reflects both systematic and nonsystematic error variation and has the same units as M_R, here reported in ksi. RE measures the systematic error or bias of the models. The definitions of these evaluation criteria are given as follows:

$$\mathrm{RMSE} = \sqrt{\frac{1}{n}\sum_{i=1}^{n}\left((M_{R-\mathrm{predicted}} - M_{R-\mathrm{measured}})^2\right)} \quad (11)$$

$$\mathrm{RE} = \frac{\frac{1}{n}\sum_{i=1}^{n}\left(M_{R-\mathrm{predicted}} - M_{R-\mathrm{measured}}\right)}{\frac{1}{n}\sum_{i=1}^{n}\left(M_{R-\mathrm{measured}}\right)} = \bar{e}/\overline{M_R} \quad (12)$$

Figure 2 shows the distribution of RMSE of evaluated models at different moisture and compaction energy condition. As expected, all the models performed well in optimum moisture and density, the condition at which was the model parameters were calibrated. Prediction errors stood the highest at dry of optimum at both compaction efforts. Figure 3, presents the prediction bias of the models on the plastic and nonplastic soils. Overall, all models underpredicted at dry of optimum for nonplastic soils.

The overall RMSE of prediction of the models per soil is shown in Table 2. The shaded cells in the table present the most accurate model. Overall, model M8—Lytton (1995) with $f_{\text{upper bound}}$—outperformed the other models in both plastic and neoplastic soils. The M2 model, which in fact is the effective stress model with f=1, performed very well for nonplastic soils, but did not provide an acceptable prediction accuracy for plastic soils. An example of the measured vs. predicted M_R by M2 for a plastic soil (PVSG) is shown in Figure 4. Table 3 shows the RE for each model and soil type. Again, model M8 was overall the most consistent model for both plastic and nonplastic soils. Model M4 and M2, while outperformed in several soil types, were erroneous in several others and did not provide a consistent prediction over the range of the evaluated soils.

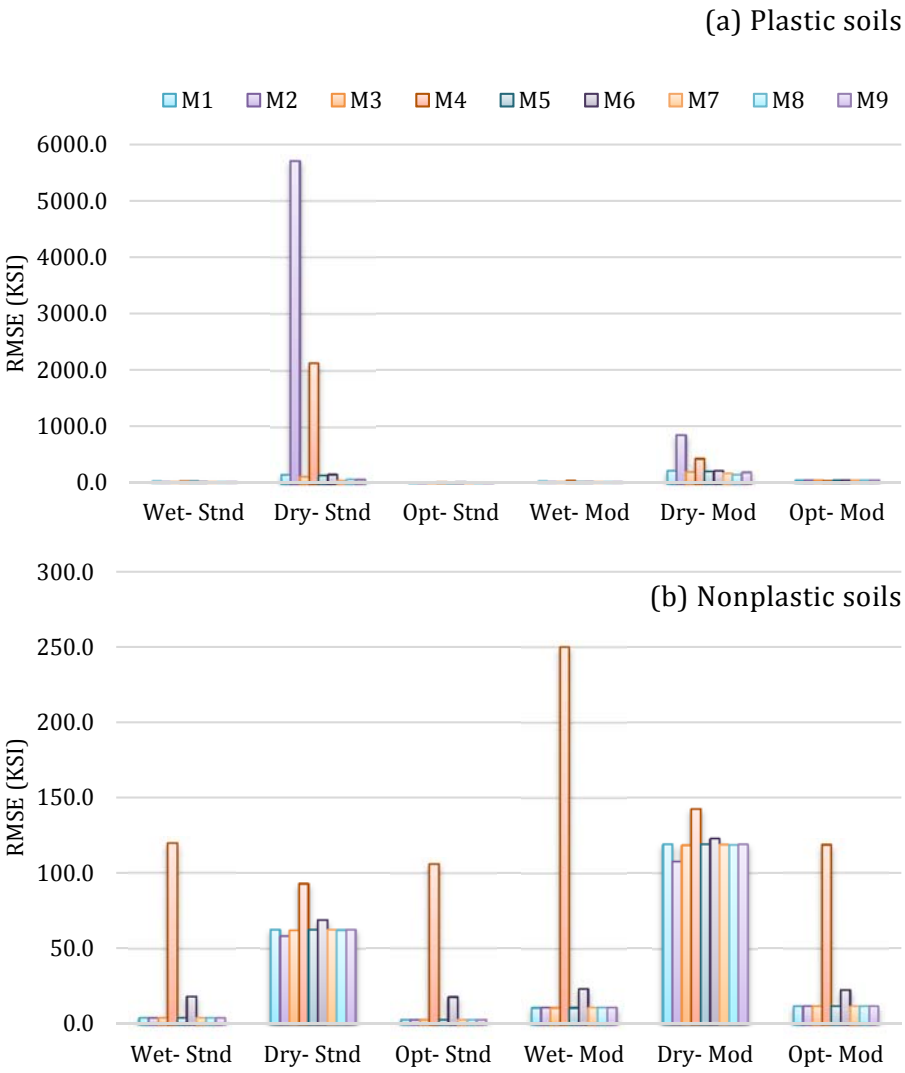

Figure 2. RMSE of evaluated models at different moisture and compaction energy condition for (a) Plastic, and (b) Neoplastic soils.

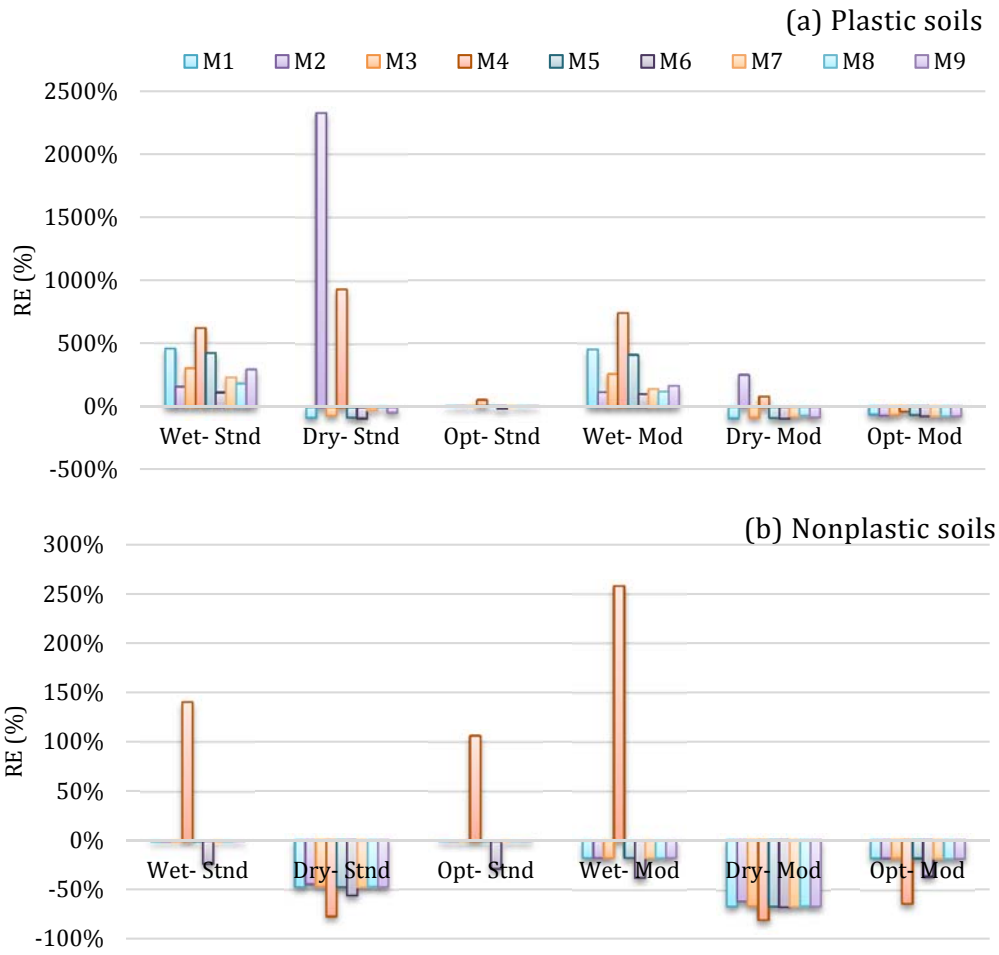

Figure 3. Average RE of evaluated models at different moisture and compaction energy condition for (a) Plastic, and (b) Neoplastic soils.

Table 2. Overall RMSE of the evaluated models for each soil.

RMSE (ksi)	M1	M2	M3	M4	M5	M6	M7	M8	M9
1.PVSG	143.0	3452.0	129.8	292.4	139.8	141.9	99.9	90.3*	118.0
2.YSSG	88.0	67.9	87.1	268.4	87.9	96.8	87.5	87.4	87.5
3.FCSG	49.6	49.6	49.2	46.2	49.7	55.0	51.4	50.9	52.1
4.SCSG	107.7	2964.4	86.9	2138.2	102.7	110.4	57.8	60.4	64.9
5.GMAB	26.9	26.8	26.9	196.0	26.9	37.5	26.9	26.9	26.9
6.SRAB	48.3	44.5	48.0	81.6	48.3	50.3	48.3	48.1	48.4
7.GLAB	41.1	39.9	40.9	67.3	41.1	43.3	41.0	40.9	41.1
8.PRAB	47.0	46.0	46.9	208.7	47.0	47.7	47.0	47.0	47.1
Plastic	100.1	2155.3	88.6	825.6	97.4	102.4	69.7	67.2	78.3
NonPlastic	50.3	45.0	49.9	164.4	50.2	55.1	50.1	50.1	50.2
All	69.0	836.4	64.5	412.3	67.9	72.9	57.5	56.5	60.8

* The shaded cells show the model yielded the lowest RMSE of prediction for each Soil type.

Table 3. Overall relative bias of the evaluated Models for each soil.

RE, %	M1	M2	M3	M4	M5	M6	M7	M8	M9
1.PVSG	-83%	1310%	-76%	85%	-81%	-86%	-53%	-30%	-68%
2.YSSG	-55%	-43%	-55%	127%	-55%	-80%	-55%	-55%	-55%
3.FCSG	-58%	-66%	-65%	-51%	-60%	-75%	-70%	-69%	-71%
4.SCSG	-71%	1789%	-58%	1240%	-67%	-83%	-21%	-5%	-35%
5.GMAB	-23%	-23%	-23%	16%	-23%	-40%	-23%	-23%	-23%
6.SRAB	-36%	-34%	-36%	-28%	-36%	-41%	-36%	-36%	-36%
7.GLAB	-32%	-31%	-32%	-36%	-32%	-38%	-32%	-32%	-32%
8.PRAB	-35%	-34%	-35%	-50%	-35%	-41%	-35%	-35%	-35%

* The shaded cells show the model yielded the lowest RMSE of prediction for each Soil type.

Figure 5 presents the RMSE and RE for model M8 at different moisture and compaction effort conditions. M8, albeit better than the other models, underpredicted the moduli at dry of optimum and optimum moisture at the modified compaction condition for all soils and overpredicted at wet of optimum for the standard and modified compaction conditions of the plastic soils.

Figure 6 shows the measured vs. predicted M_R for GMAB and PVSG for which M8 model. These two soils provided the most and least accurate predictions, respectively.

Overall, model M8—the model proposed by Lytton (1995) using the upper bound of the suction resistance factor ($\theta_w f$) based on Equations 8 and 9—was found to be the most accurate model over a wide range of fine and coarse and plastic and nonplastic soils used in pavements subgrades and bases. However, the RMSE for all models were high, far from acceptable in all the moisture and density conditions. Local biases existed in all the evaluated models. In particular, the models tended to underpredict the moduli at dry of optimum.

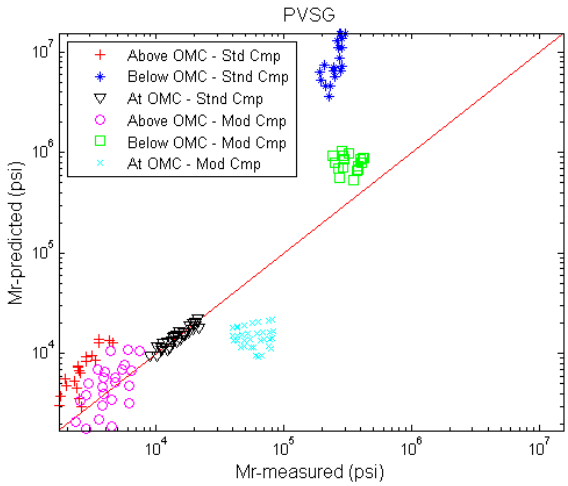

Figure 4. $M_{R\text{-predicted}}$ VS. $M_{R\text{-measured}}$ - Model M2 for Soil PVSG.

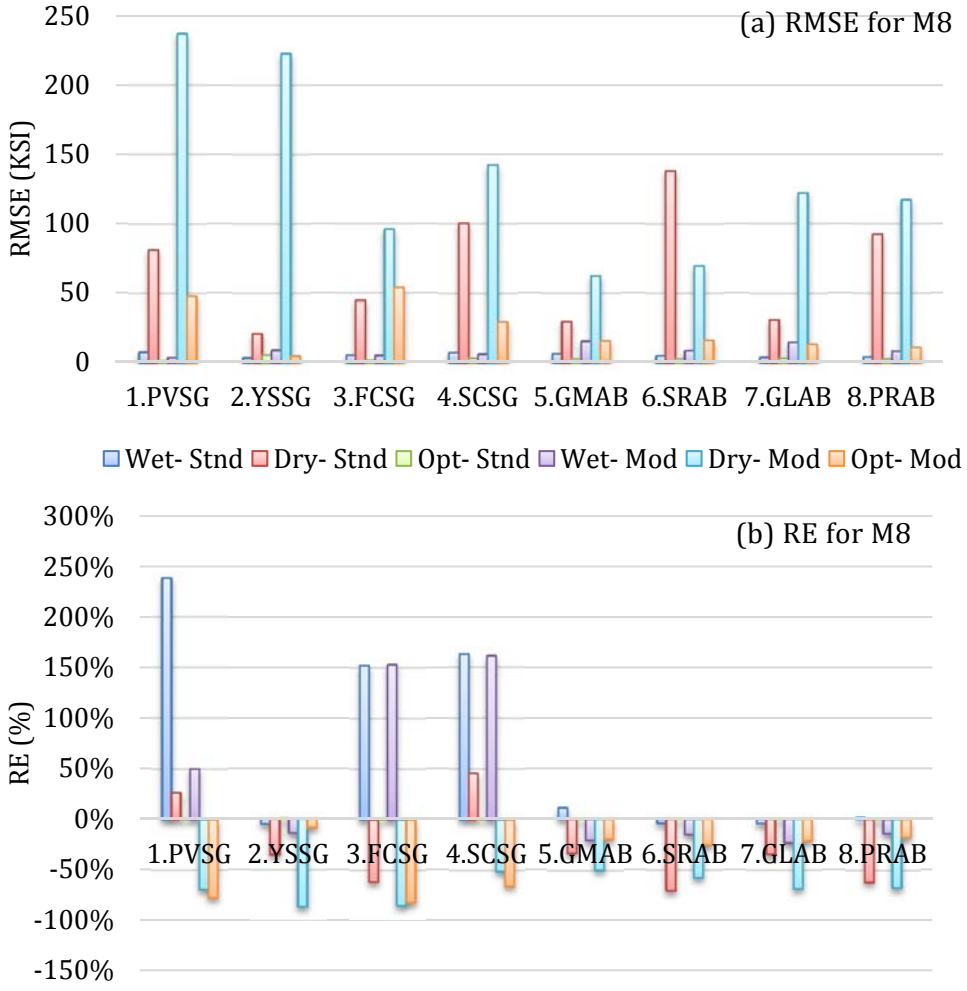

Figure 5. (a) RMSE and (b) RE at different moisture and compaction energy conditions for Model 8.

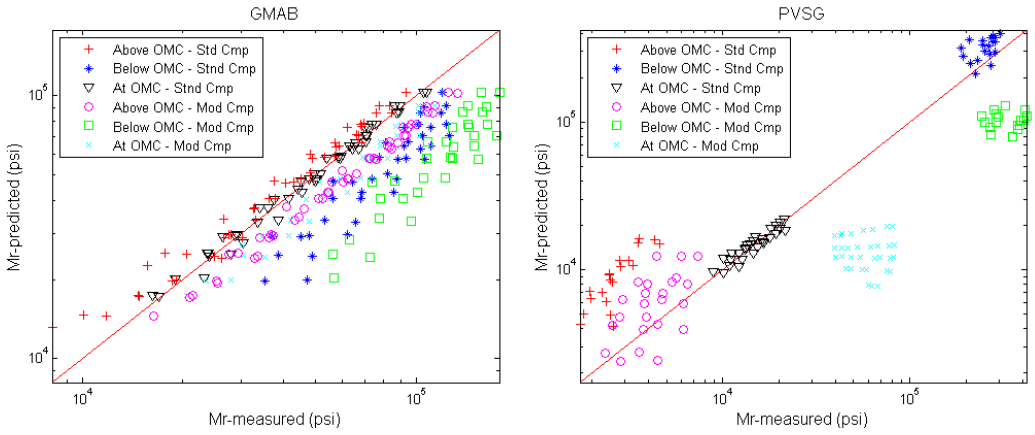

Figure 6. $M_{R\text{-predicted}}$ from model M8 VS. $M_{R\text{-measured}}$ for GMAB and PVSG soils.

CONCLUSIONS

Geomaterials in pavements are often in unsaturated condition during their service life and their resilient modulus is influenced by several factors including moisture content, density, void ratio, plasticity, and other factors. To characterize the nonlinear modulus of soils, tests at various conditions—in particular, at various stresses and moisture contents—may be required. Yet, routine testing is usually only performed at the optimum moisture and density condition. Therefore, an accurate model based on mechanics of unsaturated soils that can predict the nonlinear M_R at other test conditions is a necessity for soils characterization in mechanistic-empirical pavement design. In this study several resilient modulus constitutive models and two empirical predictive models were evaluated on independent cohesive and noncohesive soils obtained from Andrei (2003).

The statistical analysis of accuracy and bias on the predicted moduli at various moisture and density conditions found that the model proposed by Lytton (1995), designated in this paper as model M8, provided the most accurate predictions of the nine evaluated models. The model is rationally founded on the principals of unsaturated soil mechanics by incorporating the influence of moisture through its effect on pore suction (u) and the degree of the contribution of the suction on effective stresses ($\theta_w\ f$). Overall, the model performed better than the rest in terms of rationality, accuracy of prediction, and applicability to the widest range of cohesive and noncohesive soils.

REFERENCES:

Andrei, D. (2003). "Development of a predictive model for the resilient modulus of unbound materials." PhD diss., Arizona State University.

Bishop, A. W. (1960). *The principles of effective stress*. Norges Geotekniske Institutt.

Black, W. P. M. (1962). A Method of Estimating the California Bearing Ratio of Cohesive Soils from Plasticity Data*. *Geotechnique*, *12*(4), 271-282.

Fredlund, D. G., & Xing, A. (1994). "Equations for the soil-water characteristic curve." *Canadian Geotechnical Journal*, *31*(4), 521-532.

Gu, F., Sahin, H., Luo, X., Luo, R., & Lytton, R. L. (2014). "Estimation of Resilient Modulus of Unbound Aggregates Using Performance-Related Base Course Properties." *Journal of Materials in Civil Engineering*.

Khalili, N., and Khabbaz, M. H. (1998). "A unique relationship of chi for the determination of the shear strength of unsaturated soils." *Geotechnique* 48, no. 5.

Liang, R. Y., Rabab'ah, S., & Khasawneh, M. (2008). "Predicting moisture-dependent resilient modulus of cohesive soils using soil suction concept." *Journal of Transportation Engineering*, *134*(1), 34-40.

Lytton, R. L. (*1995).*"Foundations and pavements on unsaturated soils." *Proceedings of the first International Conference on Unsaturated Soils, unsat'95, Paris, France. 6-8 September 1995. Volume 3.*

Morgenstern, N. R. (1979). Properties of compacted soils. In *Contribution to panel discussion, Session IV, Proc., 6th Panamerican Conf. on Soil Mechanics and Foundation Engineering* (Vol. 3, pp. 349-354).

Roberson, R., & Siekmeier, J. (2002). Determining material moisture characteristics for pavement drainage and mechanistic empirical design. *Research Bulletin. Minnesota Department of Transportation. Office of Materials and Road Research*.

Siekmeier, J. A. (2011). "Unsaturated Soil Mechanics Implementation During Pavement Construction Quality Assurance." *Proceedings of 59th Annual Geotechnical Engineering Conference, St. Paul, MN*.

Terzaghi, K. (1996). *Soil mechanics in engineering practice*. John Wiley & Sons.

Uzan, J. (1985). "Characterization of granular material." Transportation Research Record 1022, Transportation Research Board, Washington, DC, 52–59.

Vanapalli, S. K., Fredlund, D. G., & Pufahl, D. E. (1999). The influence of soil structure and stress history on the soil–water characteristics of a compacted till.*Geotechnique*, *49*(2), 143-159.

Yan, K. Z., Xu, H. B., & Shen, G. H. (2013). "Novel Approach to Resilient Modulus Using Routine Subgrade Soil Properties." *International Journal of Geomechanics*.

Appendix C. Evaporation from Soil

The following material are largely taken from UNSAT user manual:

Fayer M. J., "UNSAT-H Version 3.0: Unsaturated Soil Water and Heat Flow Model Theory, User Manual, and Examples", Pacific Northwest National Laboratory Richland, Washington 99352, June 2000

The soil water balance equation that forms the basis of the conceptual model is:

$$\Delta S_w = I - E - T - D \quad (1)$$

in which ΔS_W is the change in soil water storage during an interval of time. Water storage is the average volumetric water content of the soil multiplied by the thickness of soil. The water balance equation simply states that the change in the amount of water stored in the soil profile is equal to the total infiltration minus the amount of water that is lost to evaporation, *E*, transpiration, *T*, and drainage, *D*.

The second step in developing the conceptual model is to identify the environmental processes and physical principles controlling each term in Equation (1). For example, the flow of heat to the soil surface affects the rate of evaporation. Based on the interrelationships among terms in Equation (1), any attempt to solve for the value of one term will be limited by the accuracy of the other terms.

Evaporation is the process of water loss from soil and/or plant surfaces to the atmosphere. Evaporation of water from the soil surface is controlled by the flow of heat to and from the soil surface, the flow of water to the soil surface from below, and the transfer of water vapor from the soil surface to the atmosphere (Hillel 1980). If any of these processes is altered, evaporation will change accordingly.

An integrated form of Fick's law of diffusion (the equation used to model vapor flow within the soil profile) addresses the interrelationships of these three processes and, therefore, has the structure necessary to predict evaporation:

$$e = \frac{c_e(\rho_{vss} - \rho_{va})}{\rho_w r_v} \quad (2)$$

in which

e = evaporation flux density, cm hr $^{-1}$
c_e = units conversion factor, cm s m $^{-1}$ hr $^{-1}$
ρ_{vss} = vapor density at soil surface, g cm $^{-3}$
ρ_{va} = atmospheric vapor density, g cm $^{-3}$
r_v = boundary layer resistance to vapor transport, s m $^{-1}$

This form of Fick's law simply states that the evaporation rate is equal to the deficit in vapor density between the soil surface and the atmosphere divided by the atmospheric boundary-layer resistance. The atmospheric boundary layer is defined as the region of the atmosphere that is directly affected by the shearing forces originating at the surface. Rosenberg et al. (1983) refer to this layer as the turbulent surface layer. Air temperature, vapor density, and wind speed are measured within the atmospheric boundary layer.

The integrated form of Fick's law accounts for the potential effects that each of the three processes identified above may have on evaporation. For the first process, heat flow, a rising soil-surface temperature causes the vapor density at the soil surface to increase. This increased vapor density, in turn, increases the vapor density deficit between the soil surface and the atmosphere, and a higher evaporation rate thus ensues. Falling surface temperature has the opposite effect of reducing the deficit, thus lowering the evaporation rate.

In the second process, water flow, a decrease in the supply of water to the surface leads to surface drying. A drier surface has a lower vapor density; hence, the vapor density deficit is smaller and evaporation is reduced. An increased supply of water to the soil surface would have the opposite effect. In the third process, both the atmospheric vapor density and the atmospheric boundary-layer resistance control transporting water vapor from the soil surface to the atmosphere. Generally, the soil surface is wetter (higher vapor density) than the air. If the atmosphere is moist, however, such as during the early morning when temperatures approach the dew point or following precipitation, the increased atmospheric vapor density decreases the surface-air vapor deficit and, therefore, decreases evaporation. Another way that the transfer of water vapor from the soil surface to the atmosphere can be reduced is by decreased wind speed or reduced eddy diffusion caused by high atmospheric stability.

UNSAT-H has an alternate conceptual model for evaporation in which the soil is isothermal. In the isothermal mode, UNSAT-H uses the partition potential evapotranspiration (PET) concept. The user supplies either daily values of PET or daily weather data, with which the code calculates daily PET values using the Penman equation. During each time step, the code attempts to apply the potential evaporation rate. If the soil surface dries to or above a user-defined matric potential limit, the time step is re-solved using a Dirichlet condition at the surface. In this situation, the surface potential is held constant at the matric potential limit and evaporation is set equal to the flux from below. For this conceptual model, the diffusion equation for evaporation can be shown to be equivalent to Penman-type equations. The Penman equation and its derivatives (Monteith 1980) are attempts to rewrite the diffusion equation to exclude the explicit dependence of the rate of diffusion on soil-surface temperature. Penman-type equations attempt to replace the need for data on soil surface temperature with information on net radiation and soil heat flux.

$$\mathrm{PET} = \frac{sR_{ni}}{s+\gamma} + \frac{\gamma}{s+\gamma} 0.27\left(1+\frac{U}{100}\right)(e_a - e_d) \quad (3)$$

where s = slope of the saturation vapor pressure-temperature curve, mb K^{-1}
R_{ni} = isothermal net radiation, mm d^{-1}
γ = psychrometric constant, mb K^{-1}
U = 24-hr wind run, km d^{-1}

e_a = saturation vapor pressure at the mean air temperature, mb
e_d = actual vapor pressure, mb.

When the soil surface is very wet, as immediately after a heavy rainfall, the evaporation rate will be at a maximum. This maximum rate, termed potential evaporation (E_p), is determined largely by atmospheric parameters that control the supply of energy to and from the surface and the transport of water vapor away from the surface. The isothermal conceptual model in UNSAT-H assumes that E_p can be calculated solely based on atmospheric parameters, thus ignoring the effects of soil surface temperature and water content on the evaporation rate.

Given this conceptual model, the actual evaporation rate from a soil surface is equal to E_p for only the few hours immediately following rainfall. More often, the evaporation rate is much lower than E_p because, as water evaporates from the soil, the soil profile begins to dry, particularly near the surface. Dry soil is a poor conductor of water and cannot readily transmit water from the moist, deeper layers to the evaporating surface at a rate sufficient to maintain the E_p rate. Thus, drying of the soil limits actual evaporation to a rate that is generally a small fraction of E_p.

At times, usually nighttime, the atmospheric vapor density can exceed the soil surface vapor density and result in the formation of dew. This form of water addition to the soil is not part of the current UNSAT-H conceptual model.

Appendix D. Laboratory experiments on soils obtained from field projects

Sample soils from the field projects were obtained for further laboratory investigations.

The conventional laboratory tests included grain size distributions based on AASHTO T27, Atterberg limits for plastic soils based on ASTM D2487, soil classification based on United Soil Classification System, and standard Proctor moisture- density curve based on AASHTO T99.

LWD measurements directly on Proctor molds were performed during Proctor compaction for three different drying scenarios.

The materials obtained from the field projects included Gravel, Sand, Silty Sand, and Clayey Sand soils obtained from US 29 Base, MD 404 subgrade, MD 424 (location 1-4) and MD 424 (locations 5-10) respectively. The grain size distributions for the evaluated soils are shown in Figure 1.

Grain size distribution

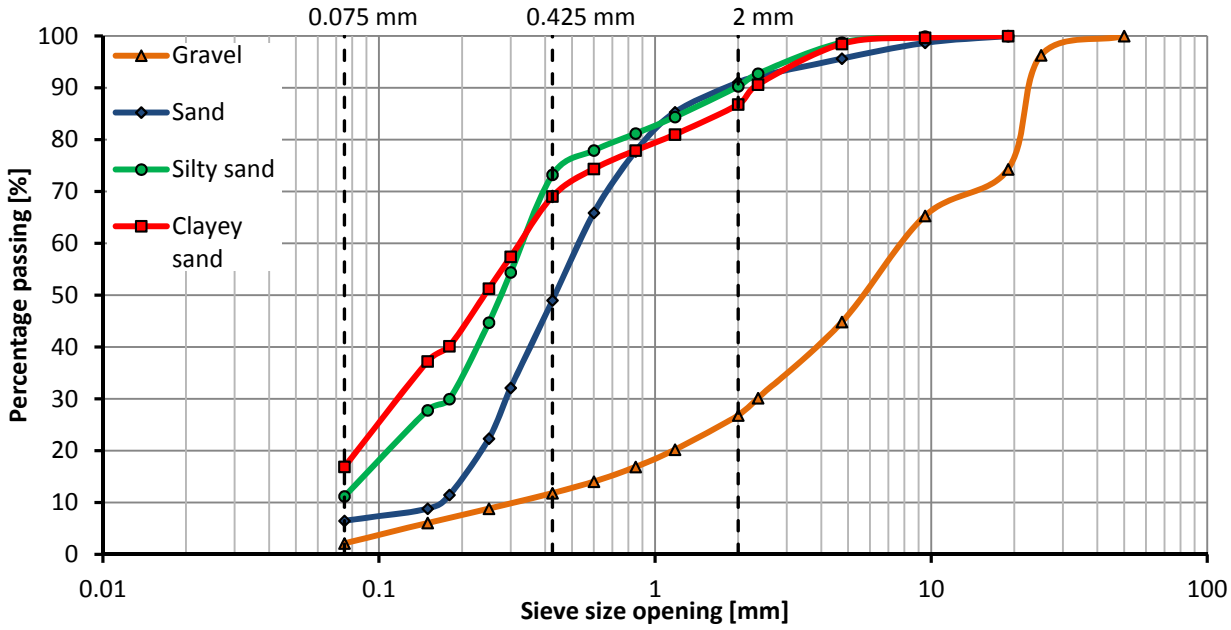

Figure 1 *Grain size curves for the analyzed soils.*

USCS soil class, coefficients of uniformity (C_u) and coefficients of curvature (C_c) are shown in Table 1. The Atterberg limits for the two fine soils are shown in Table 2.

Table 1. Coefficients of uniformity and coefficients of curvature for the studied soils

Soil	USCS	C_u	C_c
Gravel	GW well-graded gravel with sand	22.4	1.4
Sand	SP-SM Poorly-graded sand with silt	4.0	1.0
Silty-sand	SM silty sand	4.0	1.4
Clayey-sand	SC clayey sand	4.0	1.0

Table 2. Liquid limit, plastic limit and plasticity index

Type of soil	Liquid limit LL [%]	Plastic limit PL [%]	Plasticity index PI [%]
Silty-sand	22	20	2
Clayey-sand	27	22	5

Standard Proctor test

The AASHTO T99 Standard Proctor test was performed for all soils. Method D with a 150 mm mold was used for the Gravel. Method A was used for the other soils. Compaction curves based on the AASHTO T180 Modified Proctor test were provided by the contractors.

Compaction curves are presented in Figure 2 and the maximum dry density (MDD) and optimum moisture content (OMC) are shown in Table 3.

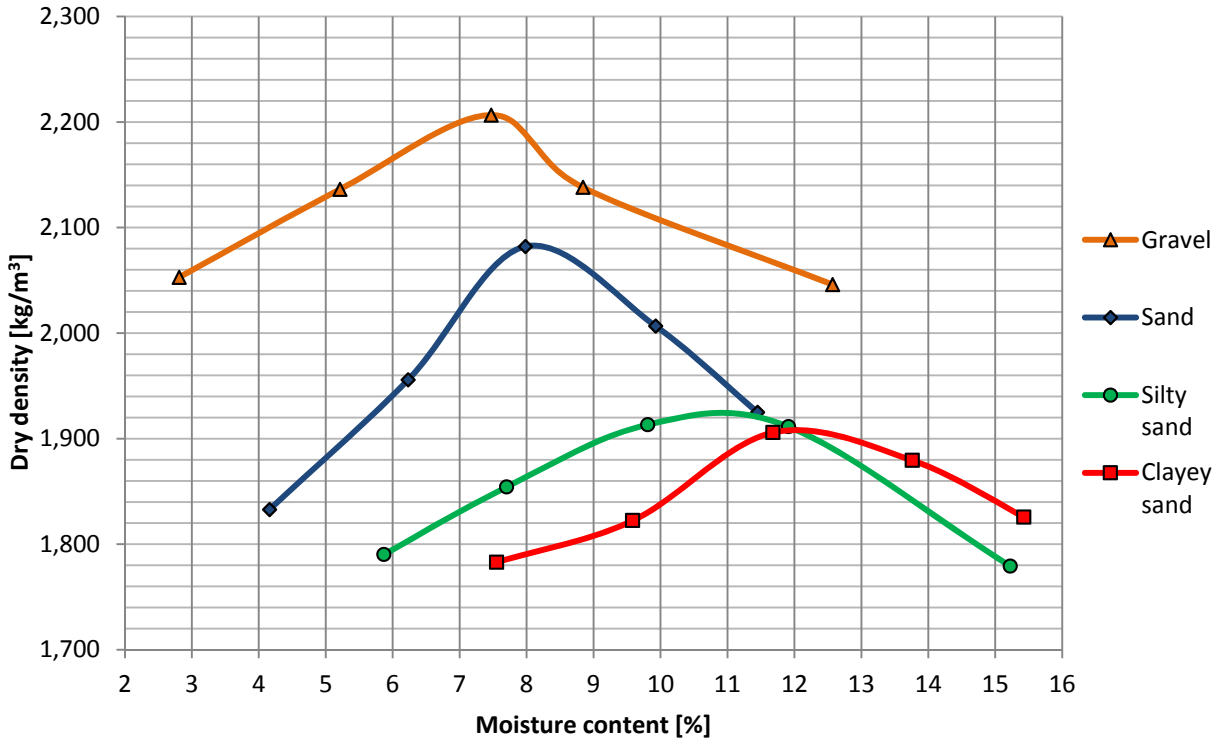

Figure 2. *Standard Proctor compaction test (AASHTO T-99) for the evaluated soils obtained from the field experiments.*

Table 3. Standard Proctor compaction test results.

Soil	OMC [%]	MDD [kg/m^3]
Gravel	7.5	2210
Sand	8.2	2082
Silty-sand	11.0	1922
Clayey-sand	12.0	1910

Light Weight Deflectometer tests on Proctor compacted samples

LWD tests were performed directly on the Proctor compacted molds on top of a concrete slab in the laboratory. The Olson LWD was used for this purpose. Similar to the field projects, six LWD drops were executed directly on the compacted soil in the mold, as shown in Figure 3. The diameter of the LWD plate was equal to that of the mold. The data from the first three seating drops were not included in the calculations. The maximum deformation (δ), and maximum impact load (F), and maximum peak stiffness (k) equal to F/δ were averaged for the last three drops and used in the analysis.

The modulus of the soil was derived from the theory of elasticity for a cylinder of elastic material with constraint lateral movement imposed by the rigid mold. In this analysis it was assumed that: (a) the soil is an elastic material, (b) the deformations occurred in the soil material only and not

in the underlying stiff concrete foundation, and (c) the impact load was static as opposed to dynamic.

The obtained equation is as followed:

$$E = (1 - \frac{2\mu^2}{1-\mu})\frac{4H}{\pi D^2}k$$

where μ = poison's ratio, H = height of the mold, D = the diameter of the plate or mold, and k = soil stiffness =F/δ as calculated by LWD device .

Figure 3 *Configuration of Olson LWD test on top of the Proctor mold.*

The tests were conducted on samples in two different scenarios:

1. Lightweight deflectometer testing concurrent to Proctor compaction test

The main objective of the test immediately after compaction was to determine the modulus curve superimposed on the dry density curve as a function of compaction moisture content.

2. Lightweight deflectometer testing during drying process

The test was conducted to study the influence of the difference between compaction and testing moisture condition on the modulus. For this evaluation, replicate samples were compacted at three different initial moisture contents using the Standard Proctor method (constant energy) based on AASHTO T99.

2.1. Drying process/ compacted at OMC.
2.2. Drying process/ compacted at OMC+2%.
2.3. Drying process/ compacted at OMC-2%.

The process was as followed:

1. Compaction of three samples at the interested initial moisture density condition according to AASHTO T-99

2. LWD measurement on one sample immediately after compaction to collect data related to the initial conditions.

3. Drying the two other samples in the Proctor mold for 8 hours and 24 hours in a controlled environmental chamber with a temperature of 25°C ± 0.5°C and relative humidity of 40-45%. Every hour the specimen was weighted and the mass was recorded in order to have a trend of the moisture loss during the drying.

4. Performing the LWD test on a soil sample after 8 hours and 24 hours of drying.

The two selected interval of time after compaction (8 hours and 24 hours) were selected to obtain a a significant moisture variation to be able to evaluate trends. Drying was limited to 24 hours, which is the assumed maximum potential delay for QA testing after compaction.

Figure 4 - Drying simulation in the environmental chamber.

Results:

The results of the first set of experiments from LWD testing concurrent to Proctor compaction test are shown in *Figure 5*.

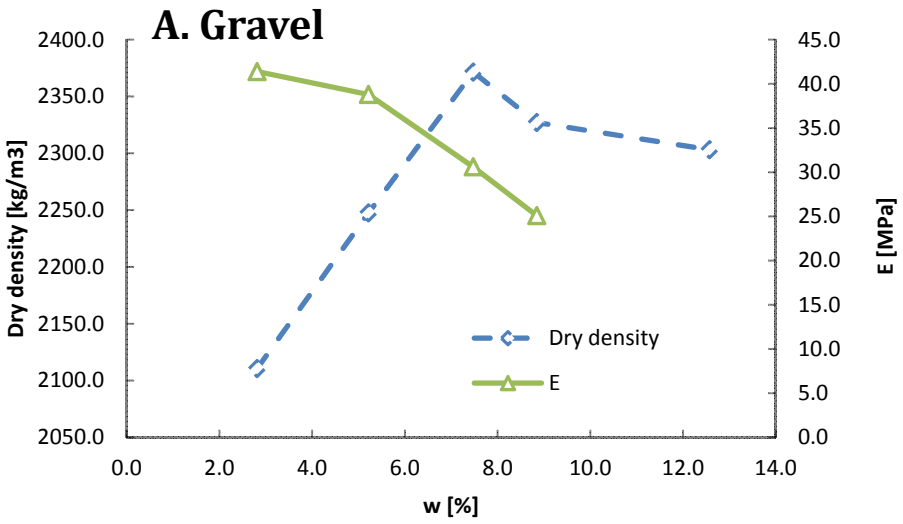
A. Gravel
Dry density [kg/m3]
E [MPa]
w [%]
Dry density
E
2400.0
2350.0
2300.0
2250.0
2200.0
2150.0
2100.0
2050.0
45.0
40.0
35.0
30.0
25.0
20.0
15.0
10.0
5.0
0.0
0.0
2.0
4.0
6.0
8.0
10.0
12.0
14.0

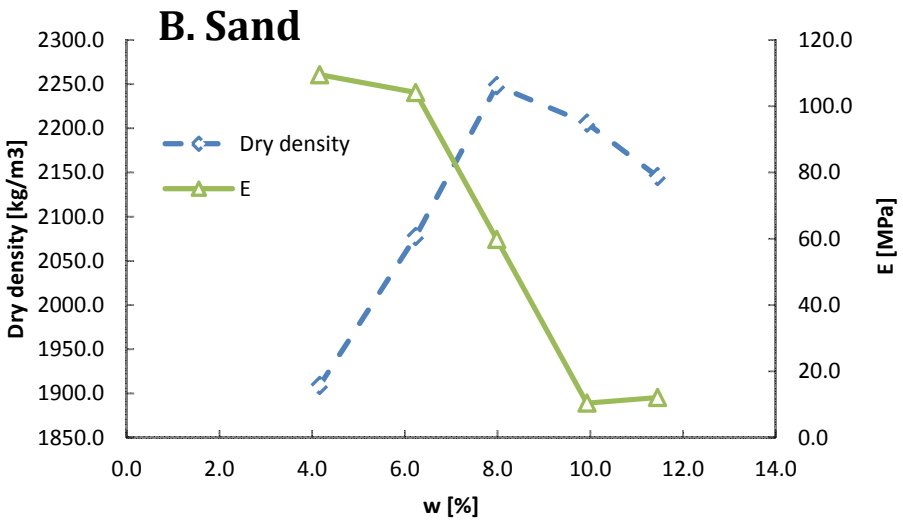
B. Sand
Dry density [kg/m3]
E [MPa]
w [%]
Dry density
E
2300.0
2250.0
2200.0
2150.0
2100.0
2050.0
2000.0
1950.0
1900.0
1850.0
120.0
100.0
80.0
60.0
40.0
20.0
0.0
0.0
2.0
4.0
6.0
8.0
10.0
12.0
14.0

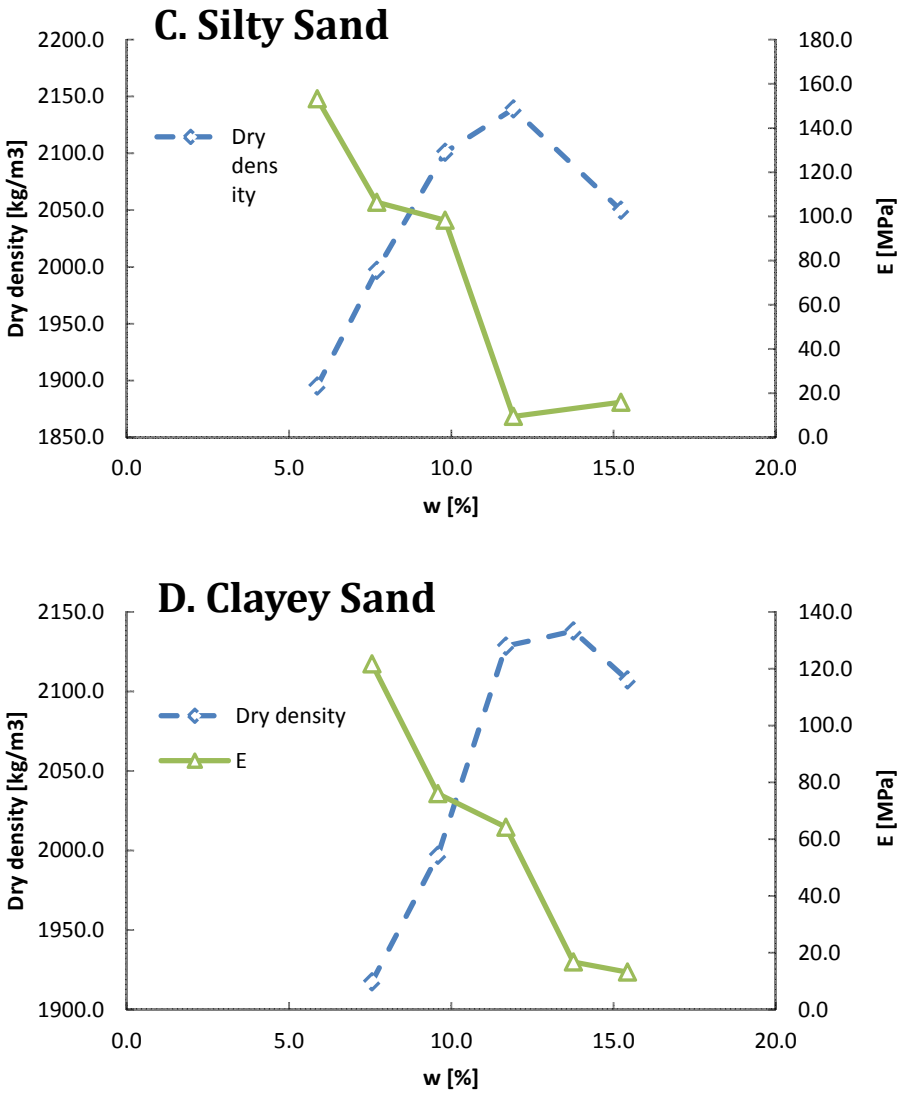

Figure 5 - Stiffness versus moisture content relationship for: A. Gravel; B. Sand; C. Silty sand; and D. clayey sand.

Preliminary observations from these results are as follows:

1. Generally, the stiffness decreases as the moisture content increases.
2. Of particular interest is the fact that the slope of modulus reduction is very steep around the OMC.

LWD testing during drying process

The objective of this study was to quantify the effect of drying on the modulus of soils as measured by LWD. It was of interest to see how the post compaction variations in moisture content due to drying may be different from the moisture variations during compaction in term of their effect on modulus.

When the compacted soil dries, its dry density and air voids remains constant while the wet density, moisture content, and degree of saturation decreases.

The following figures show the test results for each soil in detail. The figures plot modulus versus moisture content or modulus versus degree of saturation.

It can be inferred from the results that for most of the soils, especially the fine grained soils, the drying curves approximately overlapped the curve created during Proctor test, demonstrating that density has minimal effects on the modulus. The influence of testing moisture content after drying was generally similar to that of the compaction moisture content.

This study is ongoing and a larger variety of soils and test replicates will be studied. If the Proctor modulus curve overlaps with drying curves, the LWD testing concurrent to the moisture-density relationship construction can be used as a tool for setting the target values in the field for LWD testing right after compaction or after a few hours of drying.

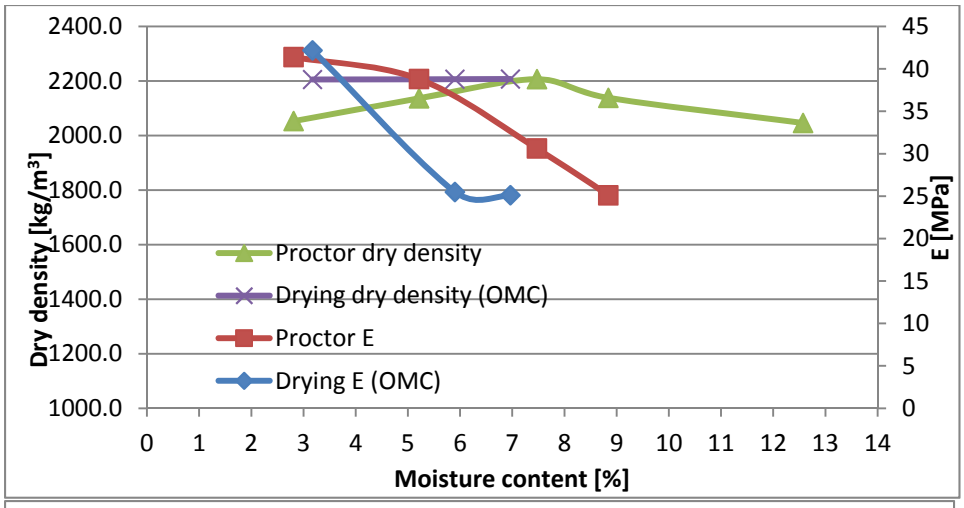
Dry density [kg/m³]
E [MPa]
Moisture content [%]
Proctor dry density
Drying dry density (OMC)
Proctor E
Drying E (OMC)

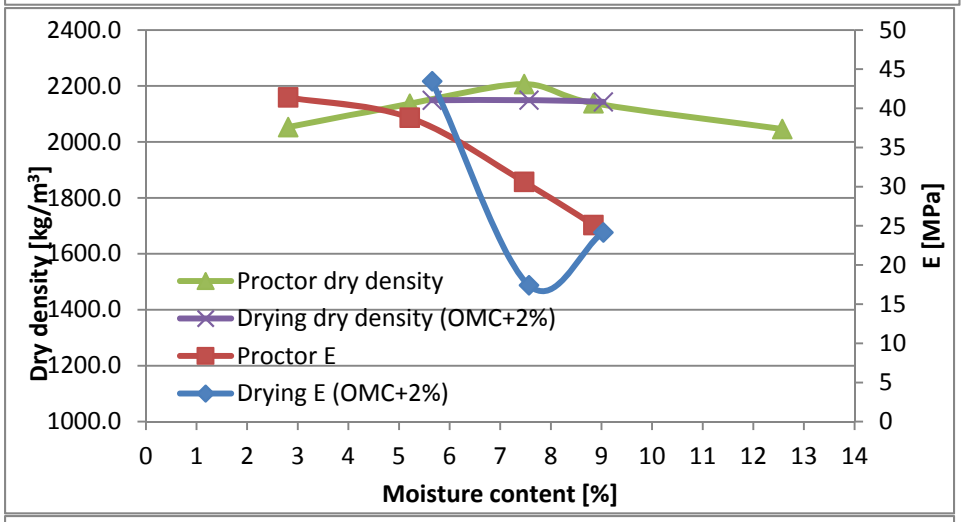
Dry density [kg/m³]
E [MPa]
Moisture content [%]
Proctor dry density
Drying dry density (OMC+2%)
Proctor E
Drying E (OMC+2%)

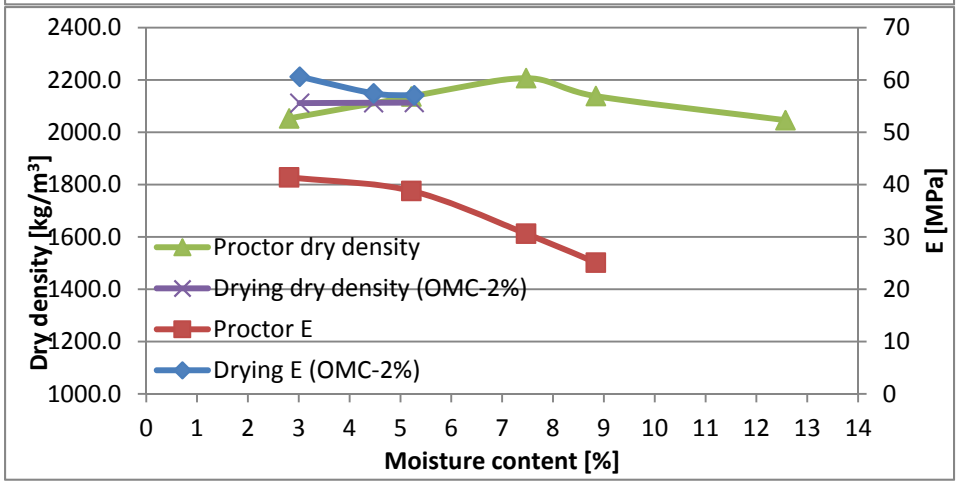
Dry density [kg/m³]
E [MPa]
Moisture content [%]
Proctor dry density
Drying dry density (OMC-2%)
Proctor E
Drying E (OMC-2%)

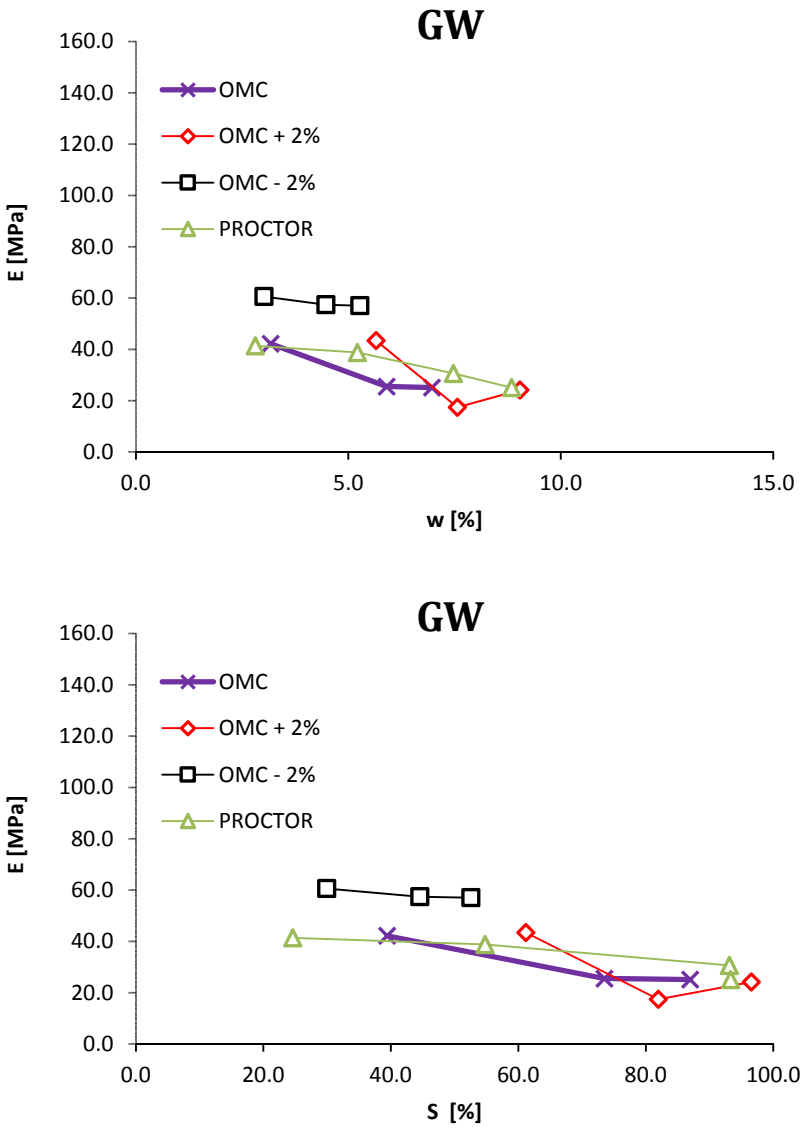

Figure 6 – Gravel Soil (GW) A. Modulus-moisture content and Density-moisture content relationships for soil compacted at OMC, B. soil compacted at OMC+2%, C. soil compacted at OMC-2%. D. Modulus-moisture content for all conditions. E. Modulus-degree of Saturation for all conditions.

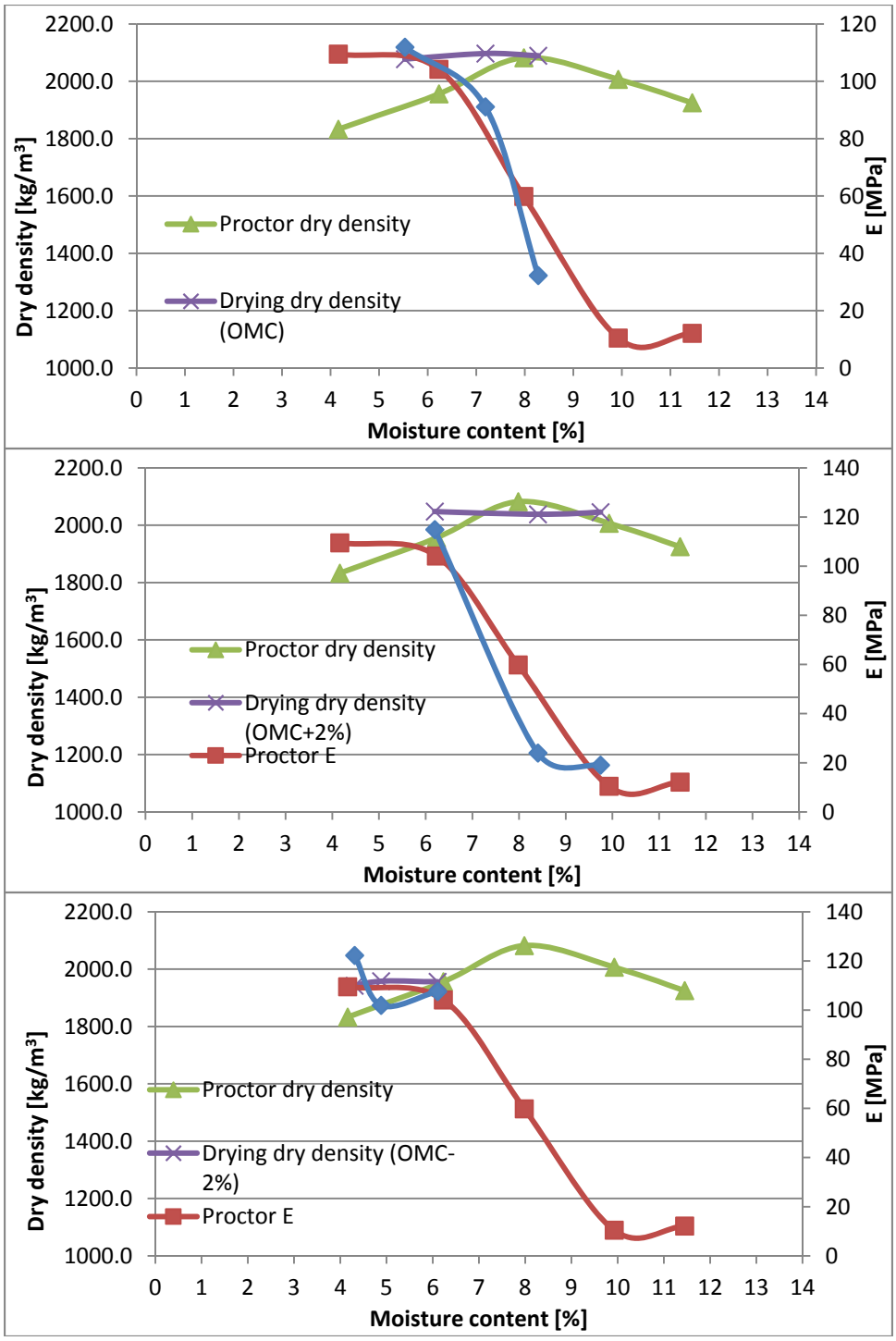
Dry density [kg/m³]
E [MPa]
Moisture content [%]
Proctor dry density
Drying dry density (OMC)
Drying dry density (OMC+2%)
Proctor E
Drying dry density (OMC-2%)

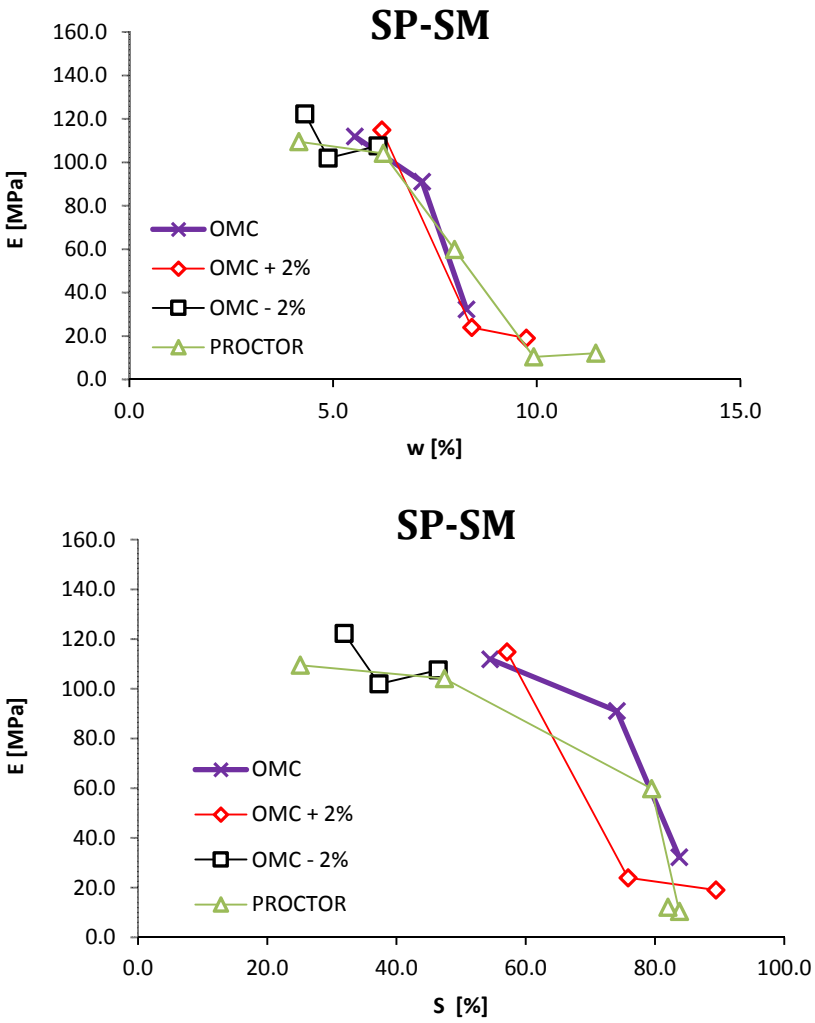

Figure 7 - Sand soil. A. Modulus-moisture content and Density-moisture content relationships for soil compacted at OMC, B. soil compacted at OMC+2%, C. soil compacted at OMC-2%. D. Modulus-moisture content for all conditions. E. Modulus-degree of Saturation for all conditions.

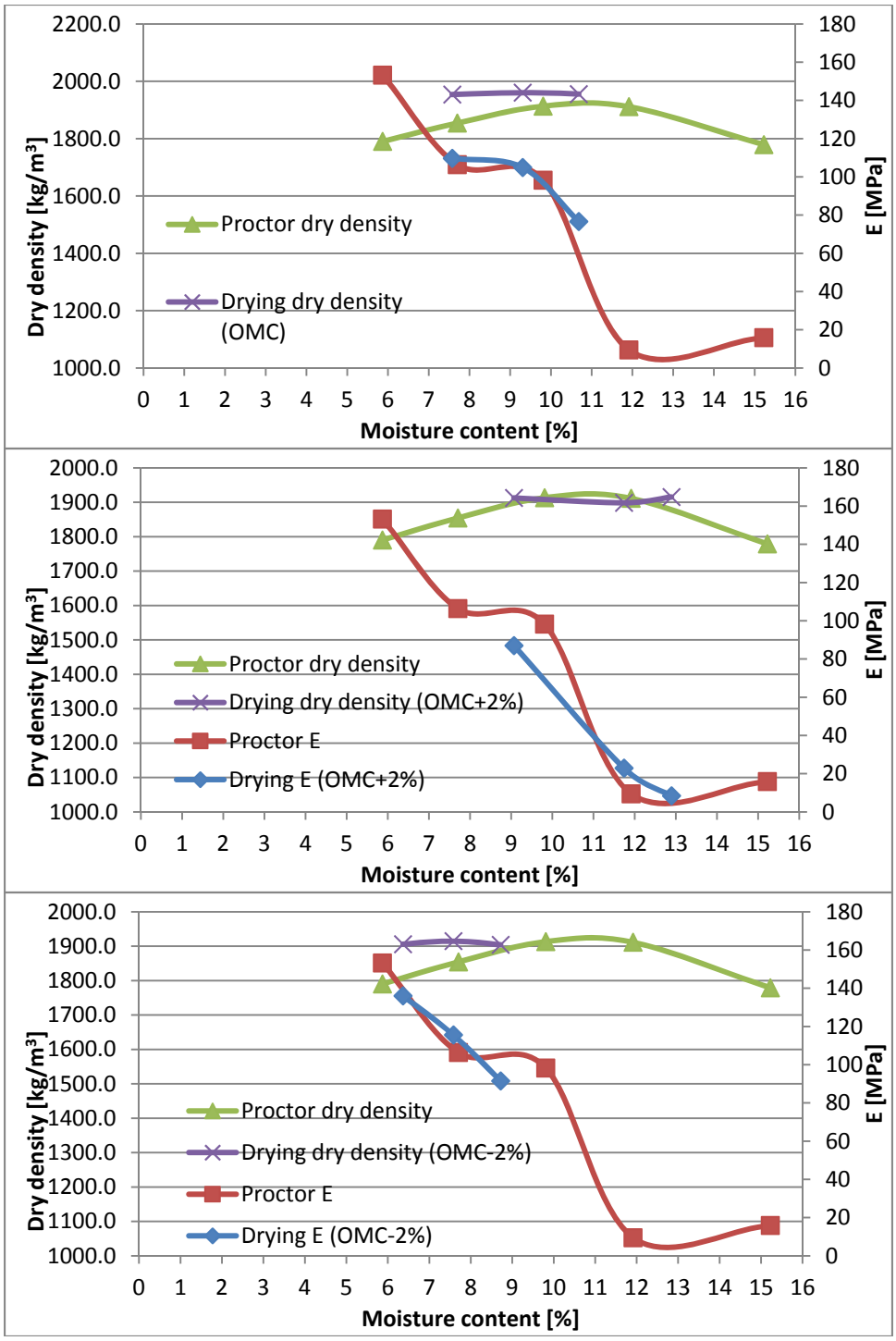
Dry density [kg/m³]
E [MPa]
Moisture content [%]
Proctor dry density
Drying dry density (OMC)
Proctor dry density
Drying dry density (OMC+2%)
Proctor E
Drying E (OMC+2%)
Proctor dry density
Drying dry density (OMC-2%)
Proctor E
Drying E (OMC-2%)

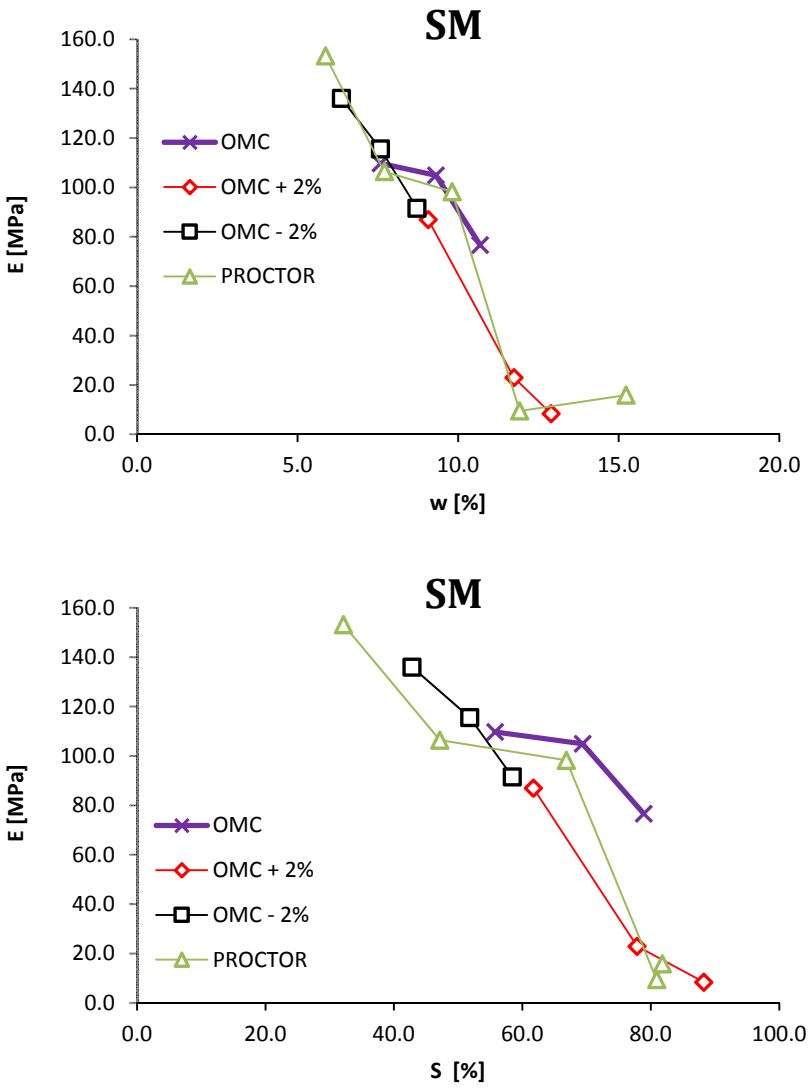

Figure8 - Silty sand (SM). A. Modulus-moisture content and Density-moisture content relationships for soil compacted at OMC, B. soil compacted at OMC+2%, C. soil compacted at OMC-2%. D. Modulus-moisture content for all conditions. E. Modulus-degree of Saturation for all conditions.

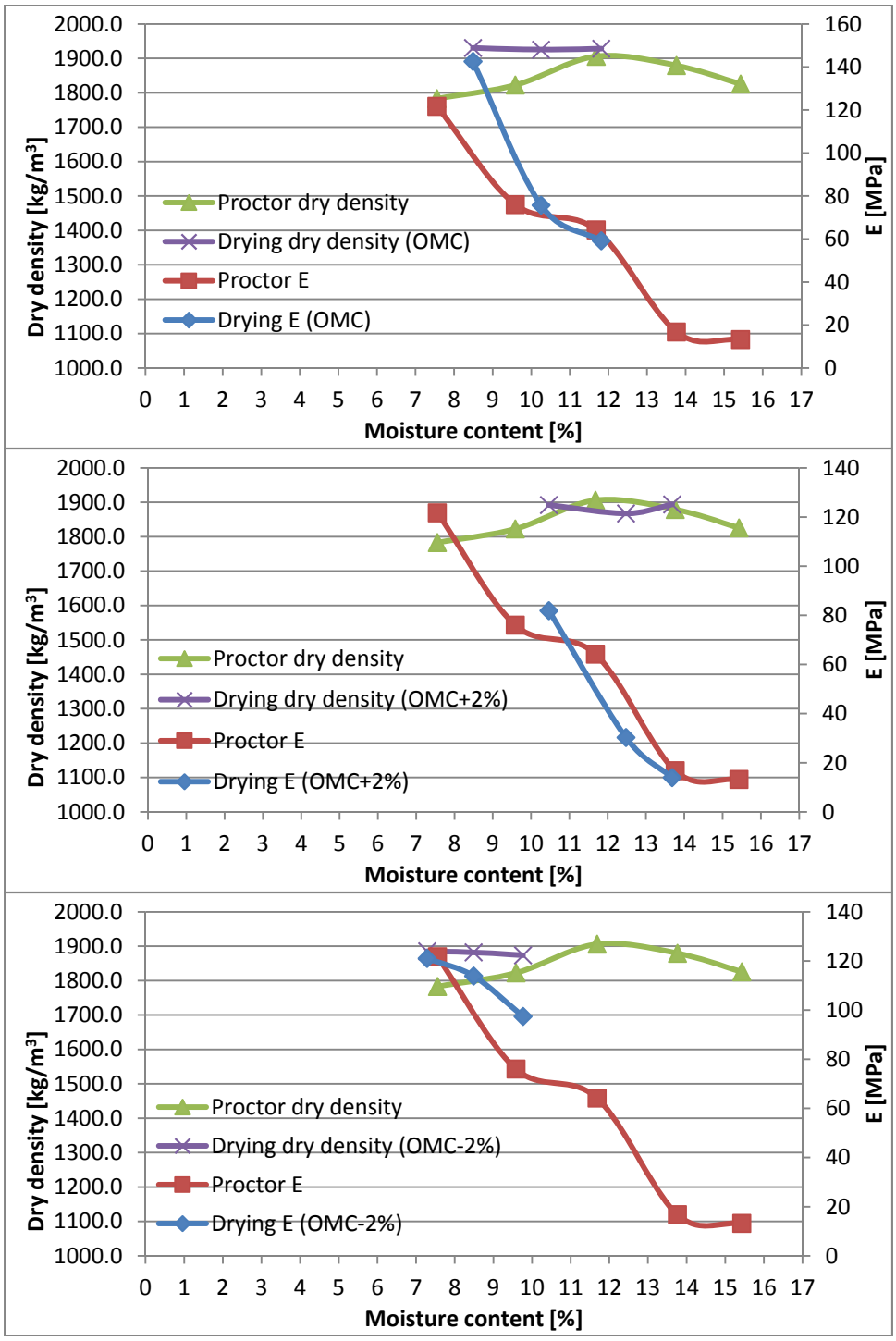
Dry density [kg/m³]
E [MPa]
Moisture content [%]
Proctor dry density
Drying dry density (OMC)
Proctor E
Drying E (OMC)
Drying dry density (OMC+2%)
Drying E (OMC+2%)
Drying dry density (OMC-2%)
Drying E (OMC-2%)

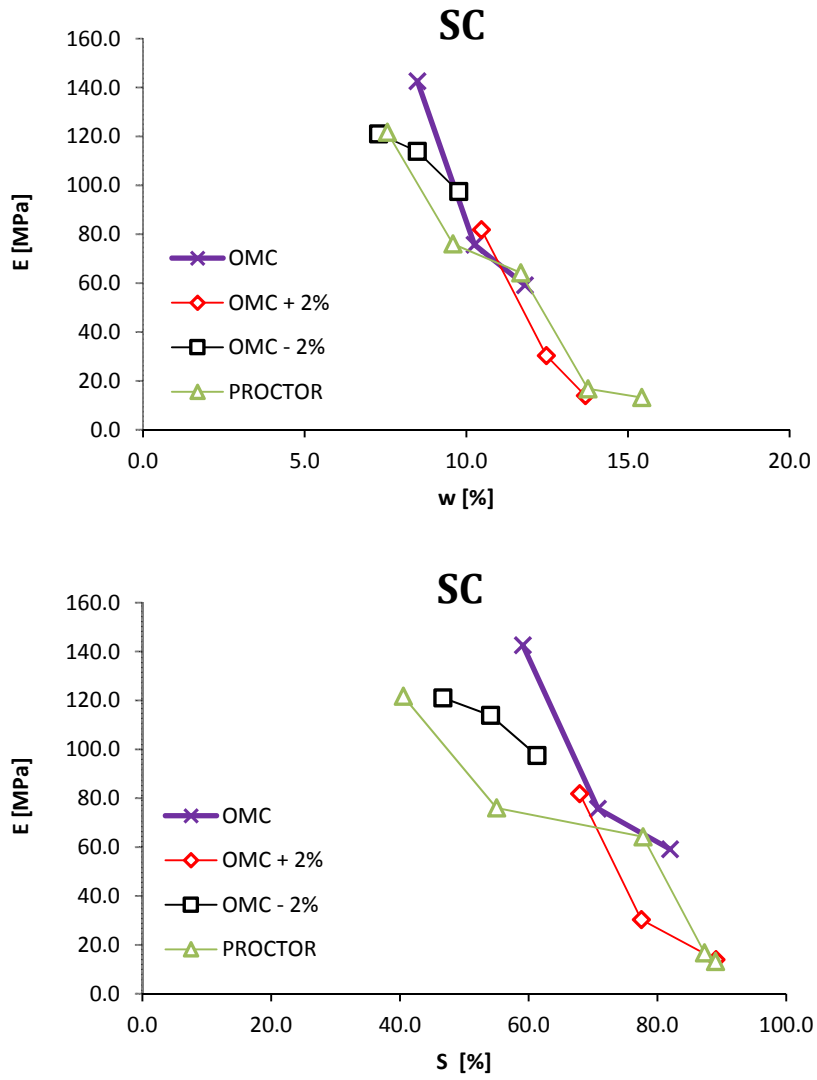

Figure 9 - Clayey sand soil (SC) A. Modulus-moisture content and Density-moisture content relationships for soil compacted at OMC, B. soil compacted at OMC+2%, C. soil compacted at OMC-2%. D. Modulus-moisture content for all conditions. E. Modulus-degree of Saturation for all conditions.

Appendix E

US 29 project

Address: US 29 NB from MD 32 to MD 175

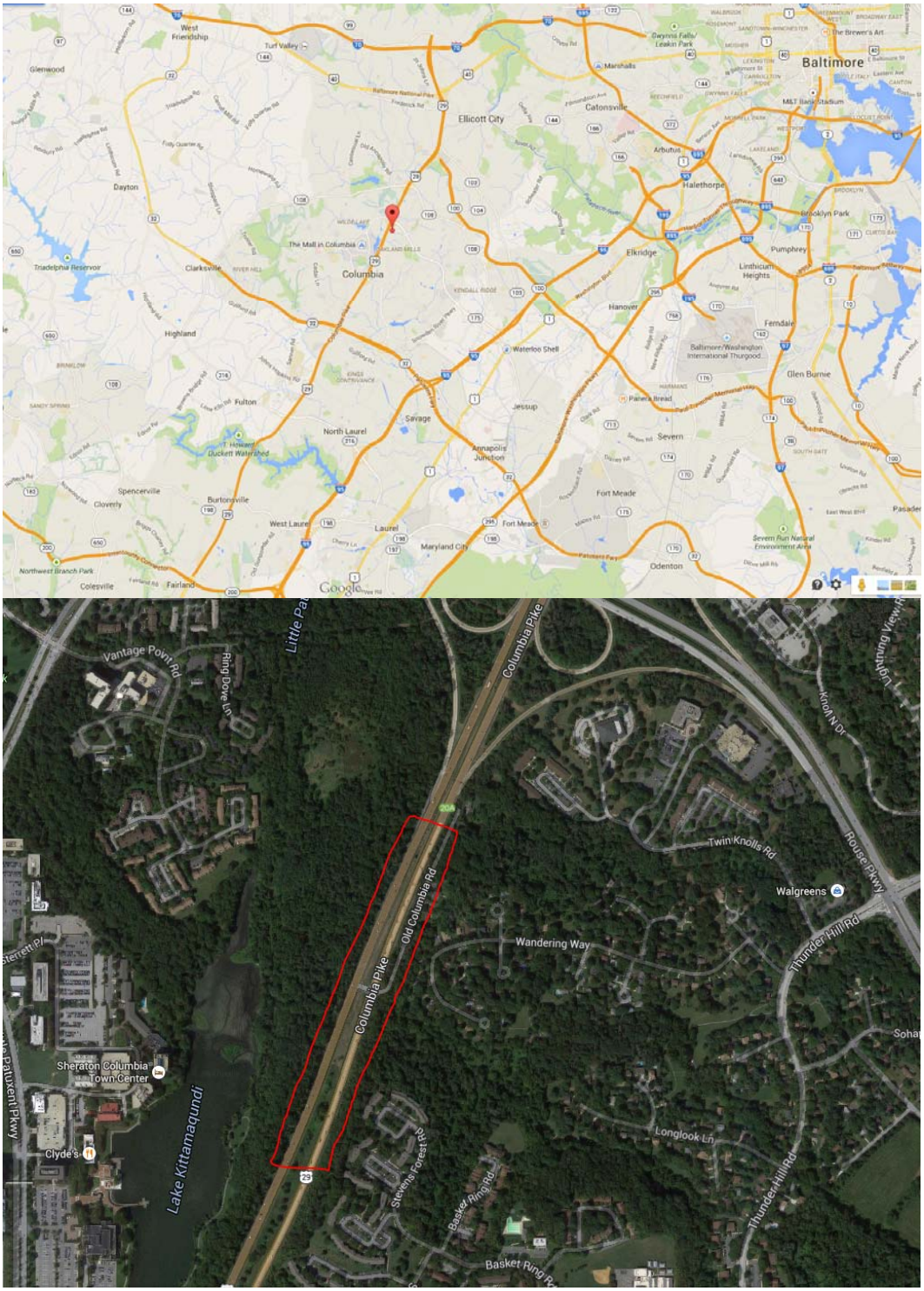

Figure 10. Project Location

Date: 10-8-14

Summary
October 8, 2014

	High	Low	Average
Temperature	**74** °F	**52.5** °F	**63.2** °F
Dew Point	**58.7** °F	**43.2** °F	**52** °F
Humidity	**97**%	**38**%	**72**%
Precipitation	**0.01** in	--	--

	High	Low	Average
Wind Speed	**14** mph	--	**3.3** mph
Wind Gust	**14** mph	--	--
Wind Direction	--	--	**West**
Pressure	**29.97** in	**29.8** in	--

Figure 11. Weather history during the testing time

The tests were performed on a 70 ft test strip on 9 test locations. The soil conditions consisted of 6 inches of Granular Aggregate Base (GAB) on top of Subgrade. The GAB material was classified as GW (well graded gravel).

Field tests included: Zorn LWD with 300 mm plate, Olson LWD with 200 mm plate, and nuclear gauge moisture and density measurements.

Figure 12. Test strip at US 29

The bousinesq equation was used to calculate the surface modulus; which is a representative of the madulus of the material in the zone of influence of the device.

$$E = \frac{2k_s\left(1-\nu^2\right)}{Ar_0}$$

Where

E = Surface modulus (ksi)

K_s = stiffness = F_{peak}/w_{peak} (kips/in)

F_{peak} = peak impact force by LWD (kips)

w_{peak} = peak induced deflection (in)

v = poison's ratio

A = stress distribution shape factor

r_0 = radius of plate

Olson 200mm/ 10 kg

Zorn	300mm/10 kg
v	0.35
A	π (uniform stress assumption)

Station #	1	2	3	4	5	6	7	8	9
MC (%)	3.8	4.1	4.3	5.4	4	5.5	4.7	4.9	4.2
DD (PCF)	133.8	137.8	139.1	137.6	144.8	130.2	138.1	133.9	135.7
WD (PCF)	138.9	144.4	145.1	145	150.5	137.4	144.6	140.5	141.4
PC (%)	93.6%	96.4%	97.3%	96.2%	101.3%	91.0%	96.6%	93.6%	94.9%
Olson200 E (ksi)	6.8	5.3	6.6	4.8	6.3	4.3	4.1	4.0	2.4
Zorn300 E (ksi)	8.8	5.5	7.9	7.3	6.0	4.9	4.7	4.2	3.0

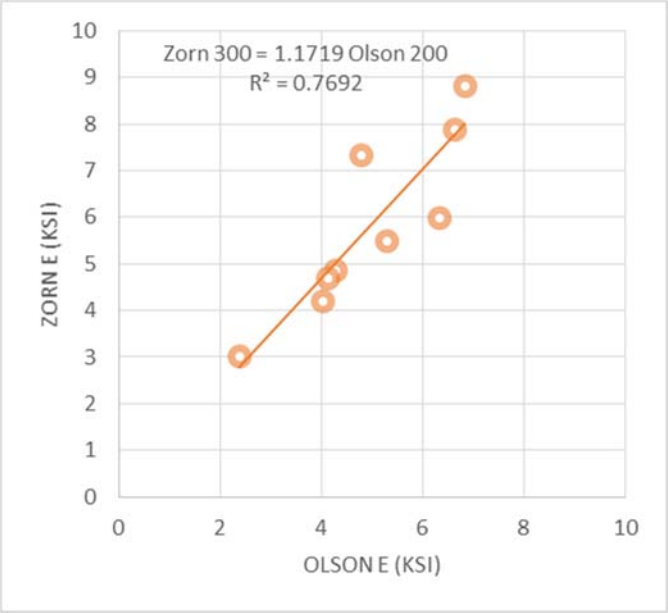

*Figure 13. Modulus (E) from Zorn LWD*300 *versus Olson LWD*200

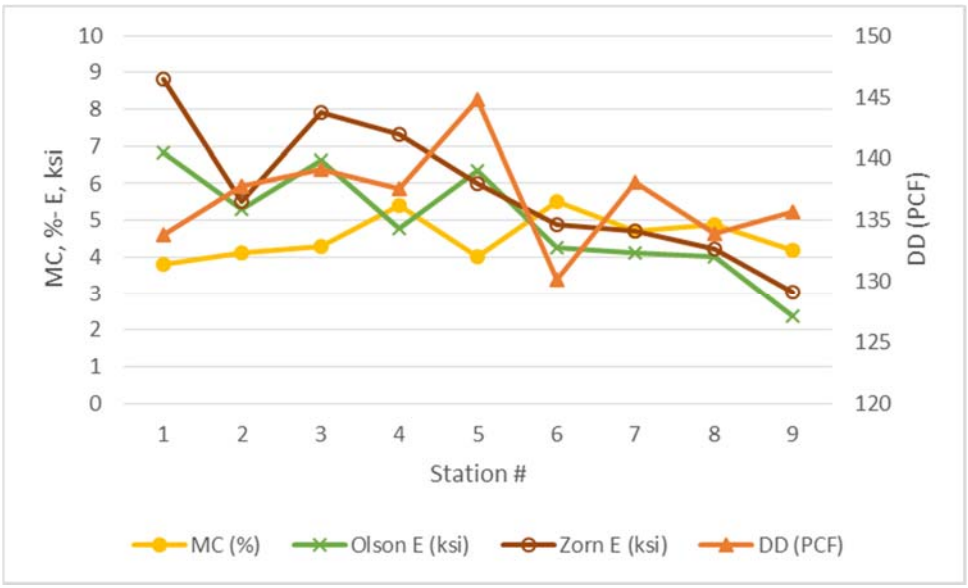

*Figure 14. Spatial variability of moisture content (MC), dry density (DD) and modulus as measured by Olson*200 *and Zorn*300*.*

MD 404 project

Figure 15. Testing location MD 404

Summary
October 10, 2014

	High	Low	Average
Temperature	**60.5** °F	**54.9** °F	**57.7** °F
Dew Point	**56** °F	**50** °F	**53.7** °F
Humidity	**96**%	**71**%	**87**%
Precipitation	**0.04** in	--	--

	High	Low	Average
Wind Speed	**2** mph	--	**0** mph
Wind Gust	**0** mph	--	--
Wind Direction	--	--	**North**
Pressure	**30.16** in	**30.07** in	--

Figure 16. Weather history during the testing time at MD 404

Figure 17. Test location- MD 404

The tests were performed on a 60 ft test strip on 10 test locations. The tests were conducted directly on the subgrade. The subgrade material was classified as SP-SM (poorly graded sand with silt).

Field tests included: Zorn LWD with 300 mm plate, Olson LWD with 200 mm plate, Geogauge, and nuclear gauge moisture and density measurements.

Figure 18. Left fig: Olson200 LWD; Right fig: Zorn300 LWD

Table 4. Assumption in calculation of LWD modulus

Olson	200mm/ 10 kg
Zorn	300mm/10 kg
v	0.35
A	π (uniform stress assumption)

Table 5. Field results

Station	1	2	3	4	5	6	7	8	9	10
MC (%)- nuk	7.3	6.5	6.3	6.3	8.6	8.5	7.4	8.3	9.5	8.3
DD (PCF)- nuk	119.8	119	120	116.2	120.9	121.3	121.3	122.7	120.5	122.7
WD (PCF)- nuk	128.6	126.7	127.6	123.5	131.4	131.7	130.3	132.9	131.9	132.8
PC based on Stnd DD*	92.2 %	91.5 %	92.3 %	89.4 %	93.0 %	93.3 %	93.3 %	94.4 %	92.7 %	94.4 %
Olson200 E (ksi)	2.13	4.40	4.40	3.51	3.97	4.29	4.30	4.48	3.48	4.21
Zorn300 E (ksi)	2.52	5.33	6.06	3.64	4.87	5.72	4.68	4.80	2.93	5.70
Geogauge (ksi)	10.41	8.73	7.75	9.34	9.24	9.87	11.41	12	8.83	11.61

* From Laboratory 5 point compaction curve performed at UMD laboratory based on AASHTO T99

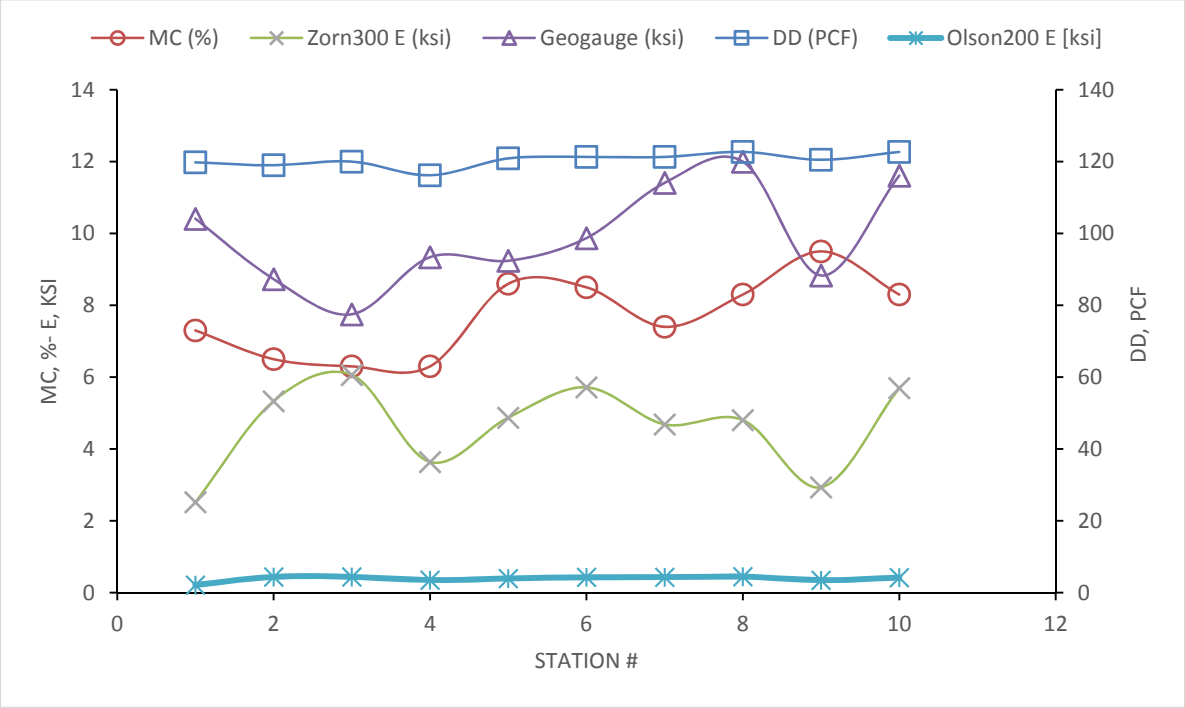

Figure 19. Spatial variation of the test results in MD 404 subgrade

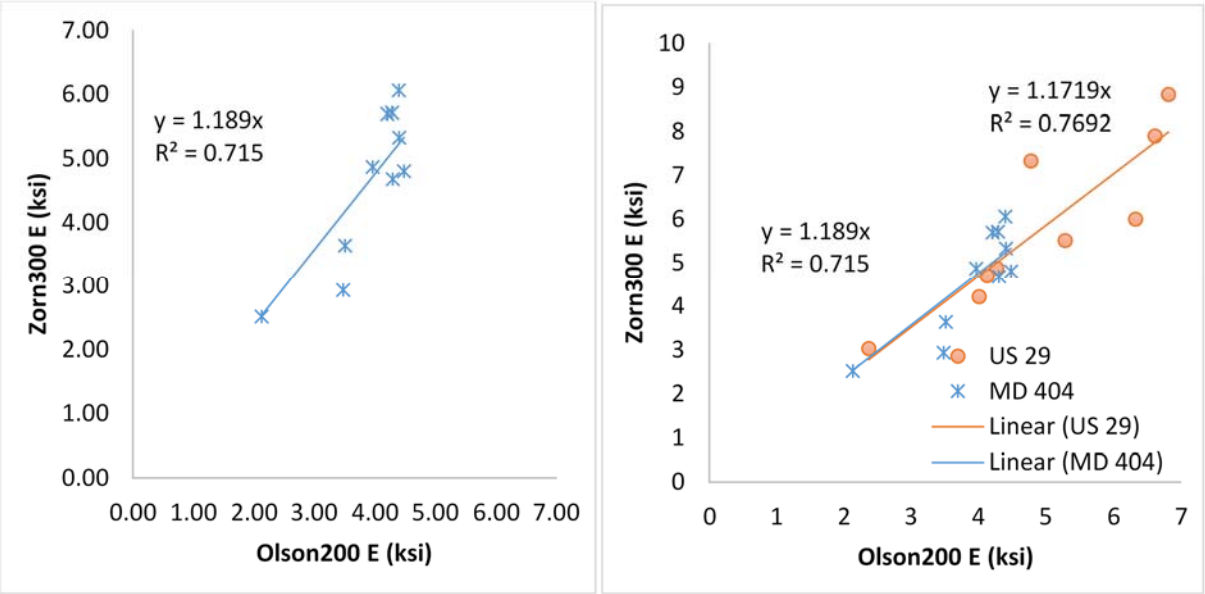

Figure 20. Modulus of Zorn300 vs Olson200. Figure in left shows the result in MD404 project only. Figure on right shows US 29 and MD 404 together.

Figure 20 suggests a very strong correlation between Zorn300 and Olson200. The modulus measured using the Zorn300 is on average 1.18 times the value measured using the Olson200.

MD424 Parking lot embankment

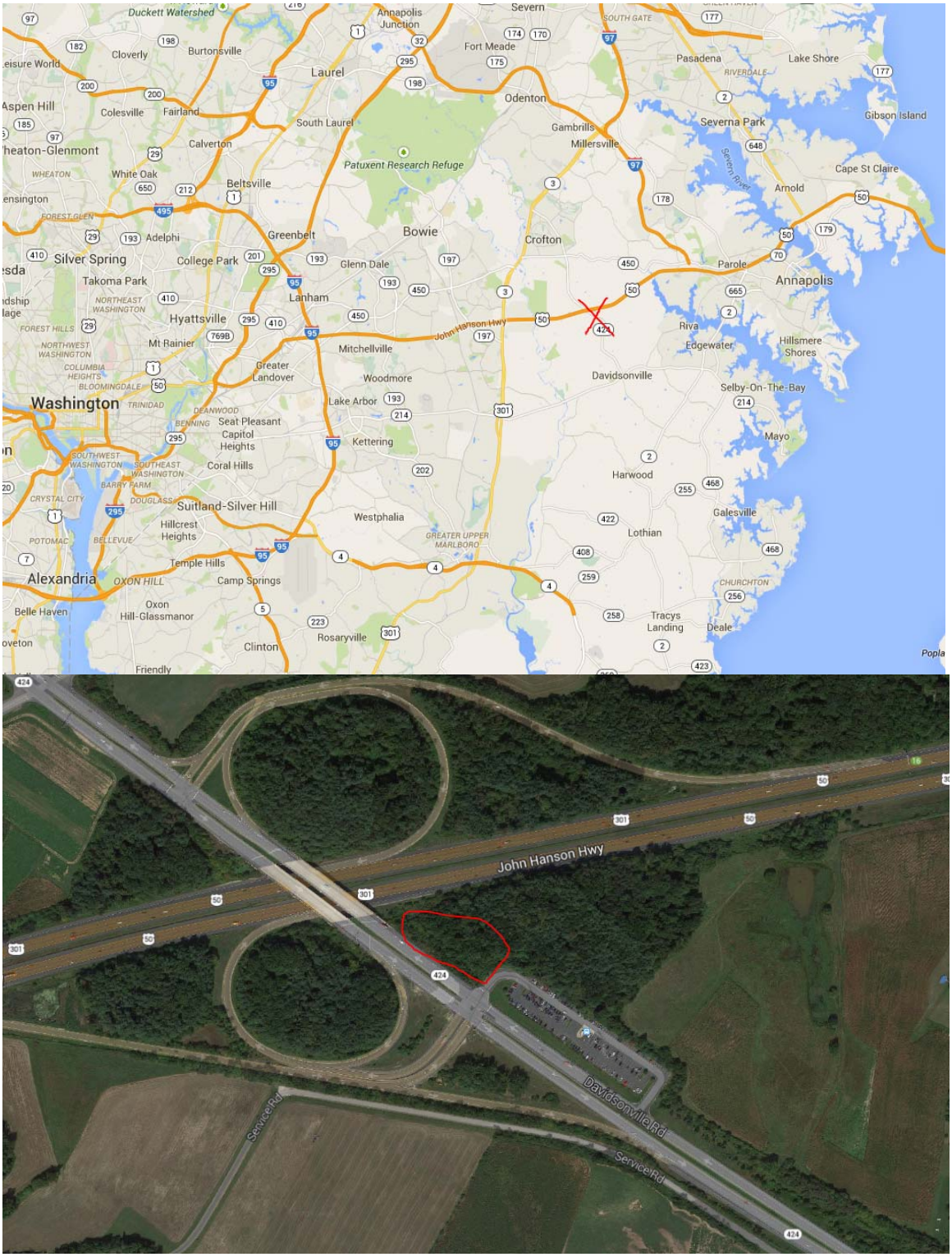

Figure 21. MD 424 parking lot embankment project location

Summary
October 20, 2014

	High	Low	Average
Temperature	**68.2** °F	**37.4** °F	**52.8** °F
Dew Point	**49.7** °F	**37.1** °F	**42.6** °F
Humidity	**99**%	**44**%	**82**%
Precipitation	**0.03** in	--	--

	High	Low	Average
Wind Speed	**7.6** mph	--	**0.6** mph
Wind Gust	**14.5** mph	--	--
Wind Direction	--	--	**South**
Pressure	**30.11** in	**29.91** in	--

Figure 22. Weather history for MD 424 project

The project was an embankment for parking lot. The earthwork soil was characterized as SM (silty sand) in test sections Section 1-4 and SC (clayey sand) in test Section 5-10.

Field tests included: Zorn LWD with 300 mm plate, Olson LWD with 200 mm and 300mm plates, geogauge, DCP, and nuclear gauge moisture and density measurements.

Figure 23. Section 1-4: SM (Silty Sand)

Figure 24. Excessive Permanent deformation observed at sections 5-10: SC soil (Clayey Sand)

Table 6

Olson200	200mm/ 10 kg
Olson300	300mm/ 10 kg
Zorn300	300mm/10 kg
v	0.35
A	4 (Inverse Parabolic Distribution on cohesive soils) 

Table 7. Field test results

Station	1	2	3	4	5	6	7	8	9	10
MC (%)- nuk	14.3	12	13.4	16.1	16.3	13.1	12.3	12.6	11.2	14.6
DD (PCF)- nuk	110.3	118.3	112.9	110	106.8	112.2	110.5	112.4	114.5	113.8
WD (PCF)- nuk	126.1	132.5	133.2	122.8	124.2	122.4	129.6	126.5	122.8	130.4
PC based on Stnd DD*	91.9%	98.6%	94.1%	91.7%	89.7%	94.3%	92.9%	94.5%	96.2%	95.6%
Olson300 E (ksi)	0.762	0.835	0.714	0.856	0.719	0.786	0.686	0.686	0.706	0.675
Olson200 E (ksi)	1.166	1.111	1.089	1.065	1.058	1.110	1.011	0.986	0.996	0.955
Zorn300 E (ksi)	1.108	0.897	0.735	0.806	0.721	0.635	0.582	0.597	0.621	0.448
Geogauge (ksi)	10.051	8.322	8.804	9.396	2.954	6.949	5.151	4.309	4.256	2.894

* From Laboratory 5 point compaction curve performed at UMD laboratory based on AASHTO T99

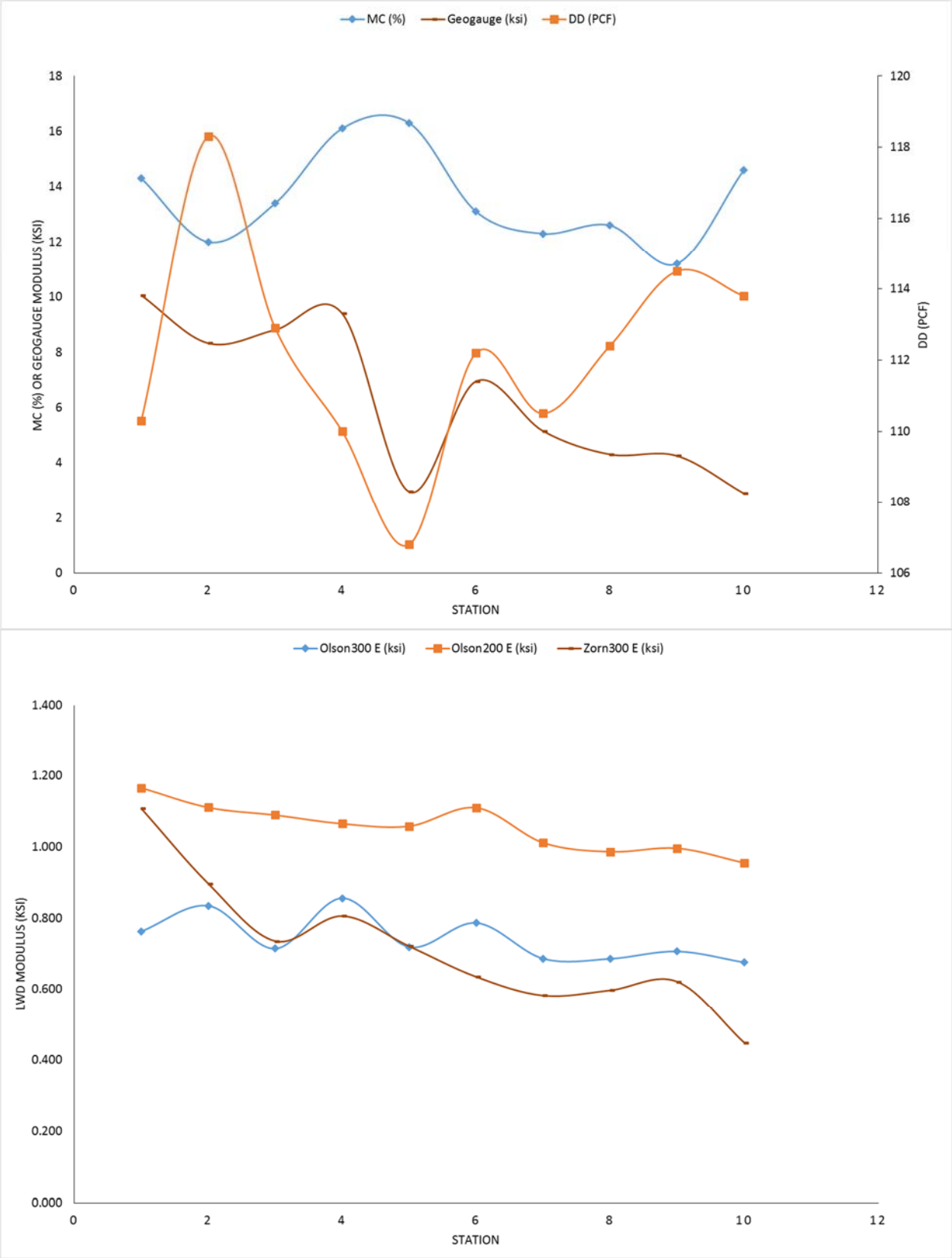

Figure 25. Spatial variability of the measured moduli

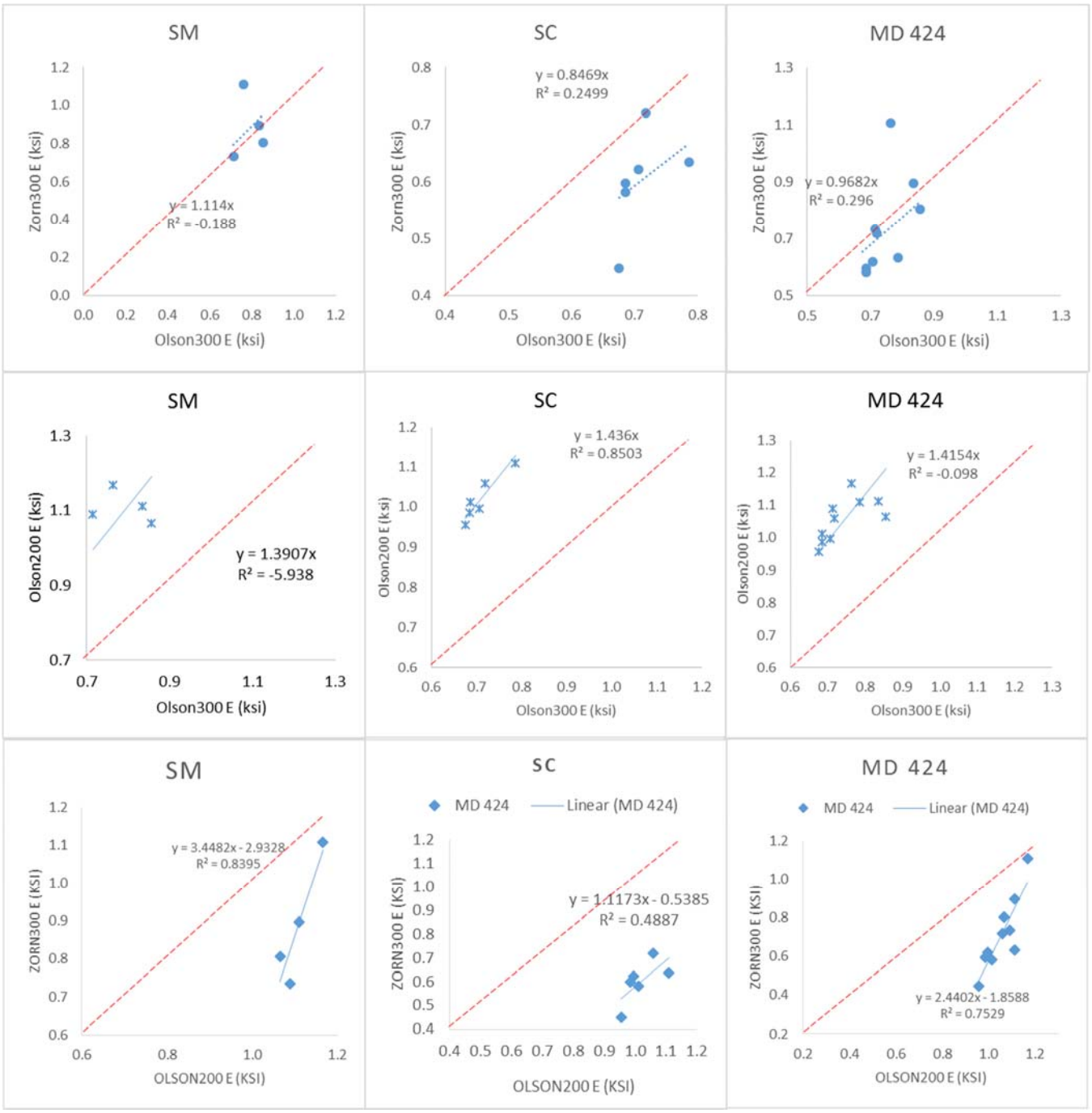

Figure 26. The correlations between various LWDs. First column, sections 1-4; second column, sections 5-10; third column all data in MD 424. Dashed line shows the line of equality

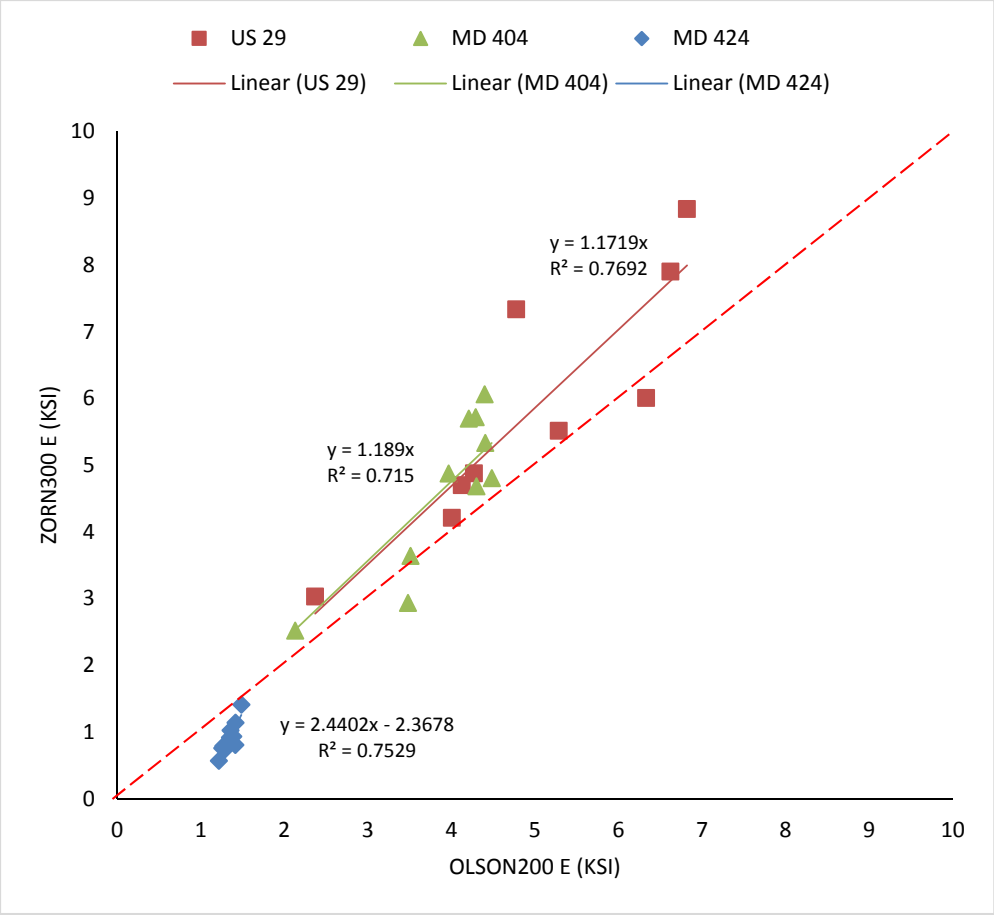

Figure 27. Surface modulus from Zorn300 vs Olson200 in all projects. Dashed line shows the line of equality

Georgia Ave

Field office location: 12250 Georgia Ave. Silver spring, MD, 20902. Tests performed included Dynatest and Zorn LWD and nuclear moisture-density gauge.

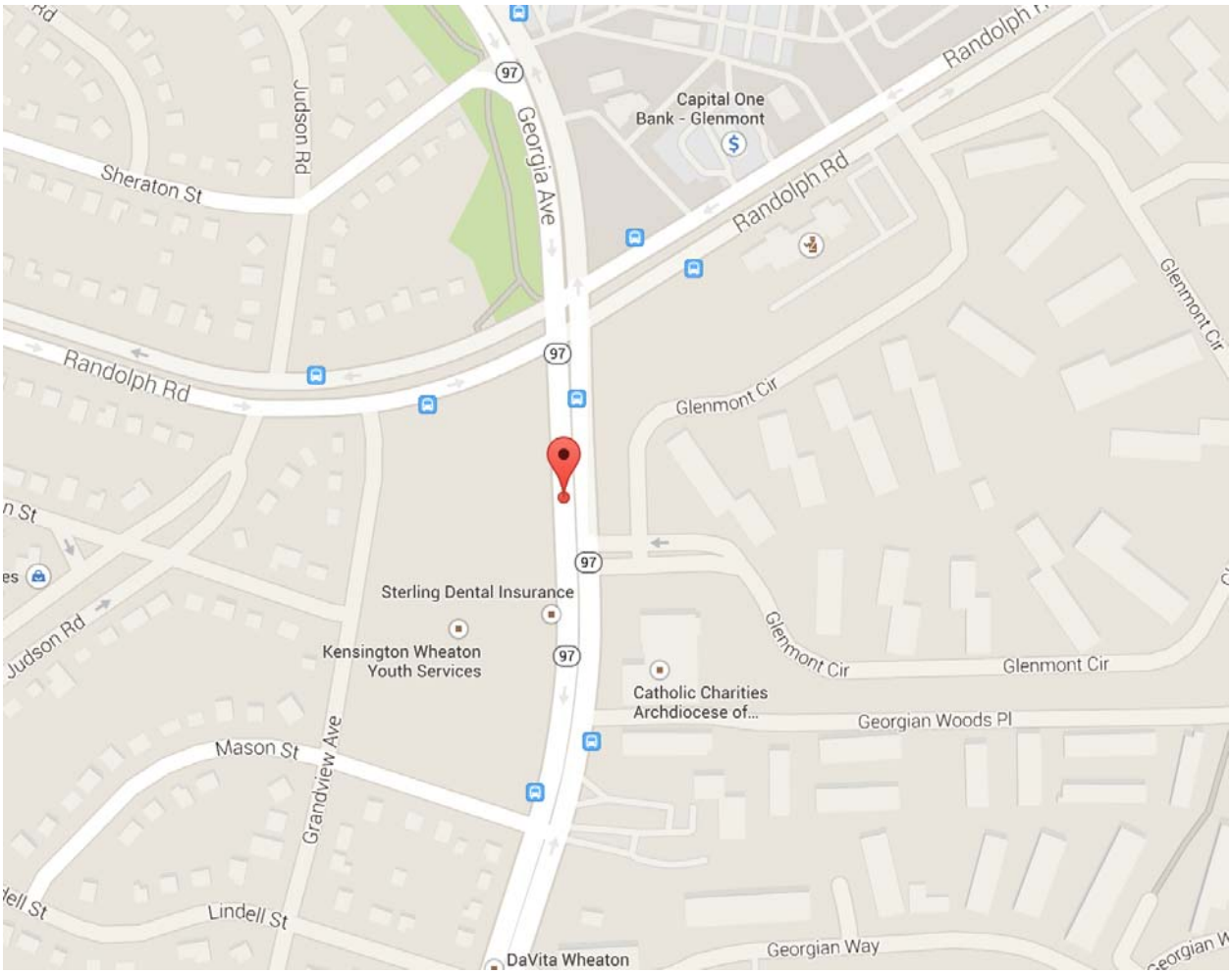

Figure 28. Site location

Weather condition

Summary
December 11, 2014

	High	Low	Average
Temperature	**39.6** °F	**33.3** °F	**36.4** °F
Dew Point	**25.1** °F	**14.9** °F	**20.8** °F
Humidity	**63**%	**39**%	**53**%
Precipitation	**0** in	--	--

	High	Low	Average
Wind Speed	**25.5** mph	--	**5.5** mph
Wind Gust	**28.9** mph	--	--
Wind Direction	--	--	**West**
Pressure	**29.93** in	**29.76** in	--

Figure 29. Georgia Ave Site

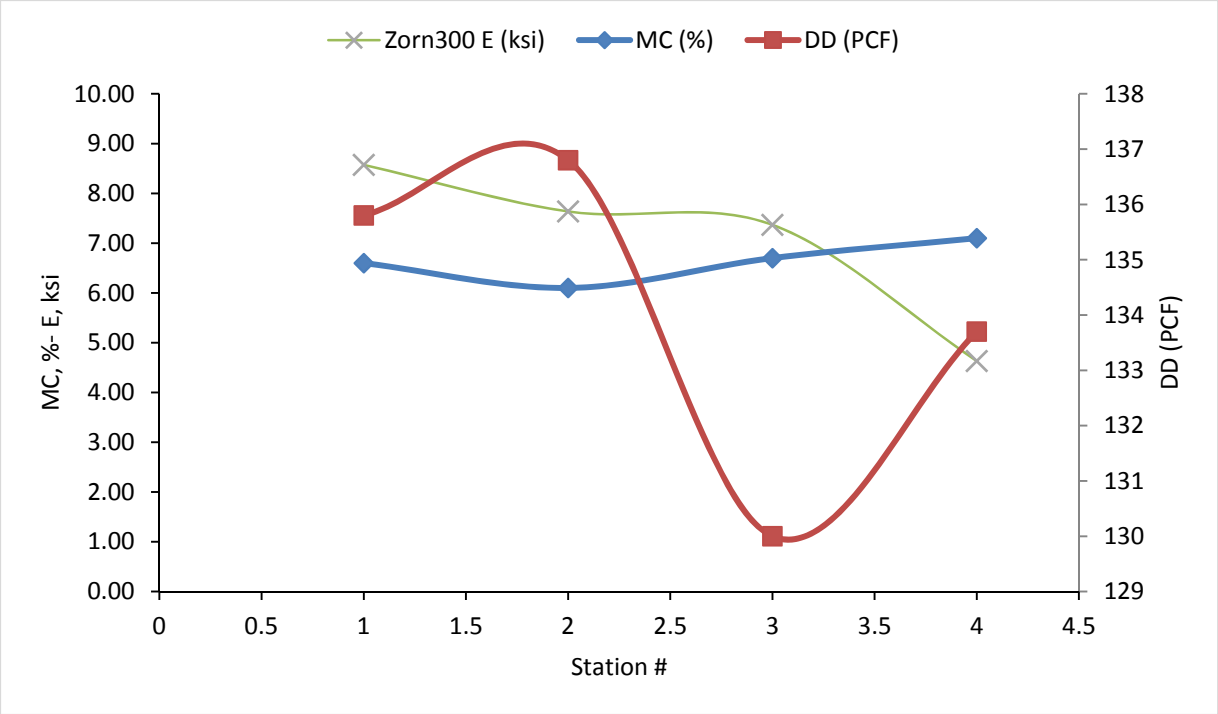

Figure 30. Spatial Variability

Station	1	2	3	4
MC (%)	6.6	6.1	6.7	7.1
DD (PCF)	135.8	136.8	130	133.7
WD (PCF)	144.7	145.2	138.5	143.2
PC based on mod DD	99.9	92.6	88.8	90.5
Zorn300 E (ksi)	8.57	7.64	7.37	4.63

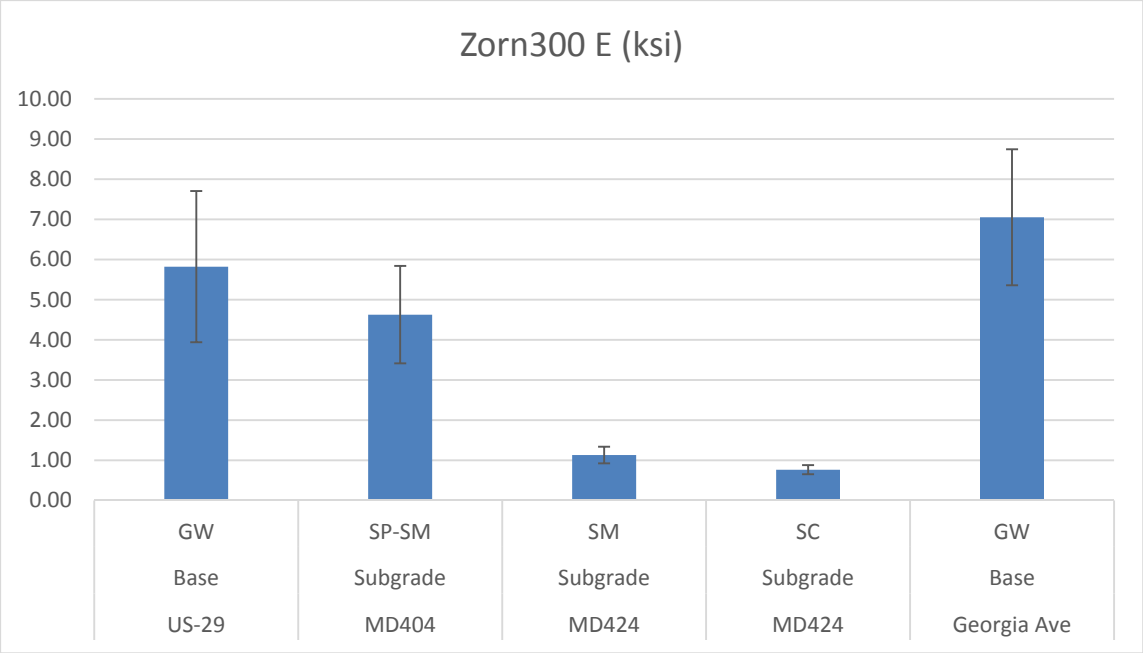

Figure 31. Average moduli at each site as measured by Zorn LWD, error bars show one standard deviation